Geometrical characterization of fracture systems using point clouds and SEFL-Software: example of the Añisclo anticline carbonate platform, Central Pyrenees

David Garcia-Sellés[1]   **Eloi Carola[2*]**   **Òscar Gratacós[2]**   **Particia Cabello[2]**   **Josep Anton Muñoz[2]**   **Oriol Ferrer[2]**

[1]Departament de Dinàmica de la Terra i de l'Oceà, RISKNAT Research Group, UB-Geomodels, Facultat de Ciències de la Terra, Universitat de Barcelona (UB)
C/ Martí i Franquès s/n, 08028 Barcelona, Spain.   Garcia-Sellés ORCID: 0000-0002-5995-5712

[2]Departament de Dinàmica de la Terra i de l'Oceà, Grup de Geodinàmica i Anàlisi de Conques (GCAC), UB-Geomodels, Facultat de Ciències de la Terra, Universitat de Barcelona (UB)
C/ Martí i Franquès s/n, 08028 Barcelona, Spain.   Carola E-mail: eloicarola@gmail.com   Carola ORCID: 0000-0003-2528-150X
Gratacós ORCID: 0000-0002-5328-9114   Cabello ORCID: 0000-0001-9291-6400   Muñoz ORCID: 0000-0003-0740-879X
Ferrer ORCID: 0000-0001-5545-9992

*Corresponding author

─┤ **A B S T R A C T** ├─

Natural fracture systems contribute significantly to rock mass anisotropies. Characterizing these systems is essential for understanding processes of fluid flow, energy exploration and storage, slope stability or tectonic processes that can affect the permeability or compaction of the material, as well as reflect its temporal evolution. This work presents a set of automatic and supervised algorithms integrated into the open-access software solution SEFL, designed to characterize fracture systems using remote sensing data sets. The software implements various strategies to quantify geometrical parameters with deterministic or stochastic descriptions, facilitating a detailed characterization of the fracture system for numerical simulations. Geological outcrops provide direct access to the rock masses and discontinuities, offering analogies with materials that are otherwise inaccessible for its direct study. The digital acquisition of the terrain using high-resolution techniques, such as Terrestrial Laser Scanner (TLS) or photogrammetry to obtain point clouds, enabled post-field studies, particularly for fracture systems that are complex, inaccessible, or large in scale. Additionally, SEFL offers a tool based on the concept of fracture stratigraphy to identify mechanical units, which are essential frameworks for measuring and calculating fracture properties. This new methodology has been applied to study the fractured Eocene limestone outcrop at the hinge of the Añisclo anticline (South-Central Pyrenees, NE Iberia) which has been digitally acquired and characterized. SEFL output data interpretations revealed an outcrop characterized by over two thousand modelled fractures, five fracture sets, fourteen fracture stratigraphic units, and 1-2 fractures/m.

KEYWORDS | SEFL Software. Natural fracture characterization. Fracture Stratigraphy Unit. Terrestrial Laser Scanner. Discrete Fracture Network.

INTRODUCTION

Natural fractures often develop complex networks whose understanding is a challenge for geosciences. A rock mass can develop fractures with an opening displacement perpendicular to the fracture surface (mode I fracture) when the tensile stress exceeds the tensile strength. This process results in secondary porosity, which is superimposed on the

primary or secondary diagenetic porosity developed prior to fracturing (LaPointe and Hudson, 1985; Peacock *et al.*, 2016; Pollard and Segall, 1987; Pollard and Aydin, 1988; Warren and Root, 1963). Moreover, this secondary porosity associated to fractures can alter the hydraulic connectivity of the rock mass, thereby affecting its absolute permeability and the effective porosity, a key parameter for fluid flow studies. These discontinuities can significantly control the mechanical and hydrological behavior of the rocks and are important for studies such as tectonic stress history, fluid flow evolution, slope stability, or underground construction projects among others.

Understanding these processes has led to the development of applications like numerical simulations as in the case of the Discrete Fracture Networks (DFNs, Einstein and Baecher, 1983). These simulations aim to enhance our understanding of behaviors associated with fracture networks. DFN uses stochastic approaches to simulate the geometrical properties of fractures (Dershowitz and Fidelibus, 1999; Einstein and Baecher, 1983; Lei *et al.*, 2017) allowing for the analysis of fracture connectivity, fragmentation assessments, upscale properties, hydrological evaluations, and simulations (Smeraglia *et al.*, 2021).

To improve the accuracy of numerical models, it is crucial to enhance the geometric characterization of the fracture model. The workflow presented in this article introduces a new tool to achieve more representative geometric characterizations using point cloud data, a specific format of High Resolution-Digital Terrain Model (HR-DTM). In general, point clouds are collected with Terrestrial Laser Scanning (TLS) devices (LIDAR technology) or through digital photogrammetry (Sørensen *et al.*, 2015; Wong, 1980) with Structure from Motion workflow (Watlet *et al.*, 2016; Wilkinson *et al.*, 2016). Integrating these advanced technologies with consolidated data obtained from field work or borehole methods can contribute to more effective solutions for fracture modelling. Quantifying parameters such as fracture position, orientation, size, and aperture (Dershowitz and Einstein, 1988; Priest, 1993) can be challenging due to the dimensions of the outcrops, their inaccessibility, or an insufficient number of surveyed fractures. The classical methodology for acquiring fracture properties from outcrops involves using a compass and tape to manually collect data. Fractures are characterized based on their intersection with a linear segment (1D scanline sampled method) drawn for this purpose or within a reference area (2D window sample method) with rectangular or circular geometry. These sampling methods require certain conditions. Firstly, the homogeneity of the mechanical behavior in the sample section of the outcrop (International Society for Rock Mechanics, 1978; Mauldon *et al.*, 2001; Priest and Hudson, 1981). Secondly, defining fracture sets that share statistically homogeneous properties. These

properties are mainly orientation but also can include other geological information such as striation or mineralization, properties not observable from lidar or photogrammetry data (Priest, 1993). Thus, the characteristics of fracture sets are part of the rock mass characterization with its geometrical properties such as: fracture spacing, vertical persistence (Gillespie *et al.*, 2001; Petit *et al.*, 1994), fracture spacing ratio (Gross, 1993), fracture spacing index (Narr and Suppe, 1991), fracture abundance parameters (Dershowitz and Herda, 1992), fractal dimensions (Bonnet *et al.*, 2001; Kulatilake *et al.*, 1997; Mandelbrot, 1982), and qualitative fracture boundedness classification and topology (Hooker *et al.*, 2013).

The mechanical behavior of a rock mass, under differential stresses, controls the process of rock fracturing at different scales (Odling, 1997; Ortega *et al.*, 2006). Although the mechanical properties can vary throughout the rock mass, sectors with similar properties can be identified and delimited as mechanical units (Corbett *et al.*, 1987; Gross, 1993; Laubach *et al.*, 2009; Underwood *et al.*, 2003). Usually, in the field, the mechanical units are determined based on visual analysis of fracture tips or by recognizing bedding boundaries, but these methods have limitations due to their simplified approaches. The identification of domains of homogeneous mechanical behavior in the field can be performed using the Schmidt hammer rebound test (Miller, 1965; Torabi *et al.*, 2010). This methodology considers Unconfined Compressive Strength as one of the main physical properties to determine the mechanical behavior of the rock. It is important to note that the measured mechanical properties reflect the present-day state of the rock mass (Olson *et al.*, 2007, 2009) which may differ from the properties at the time of fracture development. Since this time, they may have evolved by tectonic and/or diagenetic processes (Lamarche *et al.*, 2012; Laubach *et al.*, 2009; Shackleton *et al.*, 2005).

The mechanical properties of a rock mass are influenced by factors such as mineralogy, grain size, grain shape, porosity, and environmental conditions including confining pressure, pore pressure, cementation, compaction, temperature, and their historical evolution (Askaripour *et al.*, 2022; Ersoy and Waller, 1995; Gross, 1993; Nelson, 2001). In sedimentary successions, several terms are used for the characterization of the fractures. Corbett *et al.* (1987) and Cooke and Pollard (1997) define the term mechanical stratigraphy as a subdivision of rock into discrete intervals according to their mechanical properties. Gross (1993) defines a mechanical layer as a lithology-controlled unit of rock that behaves homogeneously in response to an applied stress and whose boundaries are located where changes in lithology mark contrast in mechanical properties, acting as mechanical interfaces. The term fracture stratigraphy is used to classify the rock mass into mechanical units based

on the extent, intensity, or other fracture-defining attributes, which are also named Fracture Stratigraphy Units (FSU). The boundaries of these units do not necessarily correspond to stratigraphic surfaces (Bertotti *et al.*, 2007; Hanks *et al.*, 1994; Laubach *et al.*, 2009).

The methodology described in this work for geometrically characterizing fractures begins with the massive digital acquisition of outcrop data surface. In the second stage, the acquired data are interpreted to identify fractures using the Surface Extraction From LIDAR (SEFL) Module I software (Garcia-Sellés *et al.*, 2011). In the third stage, the fractures are reconstructed with SEFL Module II (Santana *et al.*, 2012), creating a digital model of fractures that includes geometric characteristics such as fracture height, length, position, and orientation. This work introduces a new stage, SEFL Module III, where the geometric properties of the fracture sets and FSUs are parameterized and characterized. Up to date, numerous studies have presented methods based on the digitization of fracture traces from HR-DTM or digital imagery to extract different geometric properties such as fracture height, length, and orientation (Assali *et al.*, 2014; Bertotti *et al.*, 2007; Daghigh *et al.*, 2022; Geyer *et al.*, 2015; Gigli and Casagli, 2011; Hardebol and Bertotti, 2013; Hodgetts, 2013; Hodgetts *et al.*, 2007; Seers and Hodgetts, 2014; Tavani *et al.*, 2014). Other studies have dealt with automatic or semi-automatic identification of fractures from HR-DTM to measure properties (Becker *et al.*, 2018; Jaboyedoff *et al.*, 2007; Lato and Vöge, 2012; Massiot *et al.*, 2017; Olariu *et al.*, 2008; Slob *et al.*, 2005; Wüstefeld, 2018) or have combined both methodologies (Wilson *et al.*, 2011). The approaches tackle the complexity of creating a link between massive remote sensing data and technologies that require detailed fracture models such as the DFNs. The strategies presented in this work combine automated measurements with classical manual methodologies improving the geometrical characterization of fractures. Finally, due to the importance of mechanical units in rock masses, SEFL Module III includes a tool to provide more criteria for identifying boundaries based on fracture stratigraphy concept, specifically, based on the intensity of fractures. This tool has been successfully applied to the poorly-bedded carbonates of the Añisclo anticline (Central Pyrenees, NE Iberia) to characterize fold-related fractures.

METHODOLOGY

This section is organized into six subsections that review and describe the software and elements implemented in the methodology. The initial three subsections review the modules of the SEFL software for fracture surface identification (SEFL Module I), modeling (SEFL Module II), and processing for fracture characterization (SEFL Module III). The following three subsections describe the parameters and strategies implemented to identify the FSUs and characterize the fractures and fracture sets. Fractures visible through their traces on the surface of the outcrop are not modeled and, therefore, not characterized. However, the suitability of using this process must be considered according to the configuration of the fractures and outcrop surfaces. The proportion of fractures exposed as outcrop traces, or as a surface trace, must be considered to achieve suitable results.

Fracture identification (SEFL Module I)

SEFL Module I processes HR-DTM to semi-automatically identify outcropping fracture surfaces that have been acquired digitally with sufficient resolution and accuracy to be modeled at the desired working resolution (Garcia-Sellés *et al.*, 2011). TLS facilitates the rapid and efficient acquisition of a large volume of georeferenced data points from an outcrop, resulting in more accurate and reliable HR-DTMs (input data, Fig. 1) compared to the more economical and easy-to-use digital photogrammetry Structure from Motion workflow. The acquisition process is designed to mitigate outcrop occlusions or shadowed zones (Sturzenegger and Stead, 2009).

The SEFL Module I algorithms fit normal vectors at each point of the HR-DTM. The process selects, for each point, surrounding points inscribed in a sphere of user-defined radius (vectorizing process of Module I, Fig. 1) to adjust the normal vector to the plane defined by the selected points. Each normal vector is calculated based on the eigenvector method using the moment of inertia analysis enabling the calculation of the orientation and indices of collinearity and coplanarity (Fernández, 2005; Woodcook, 1977). The indices of collinearity and planarity, as well as the difference between the normal vectors, and a minimum number of points, determine the creation of a cluster of points modeling a fracture. These factors are defined by the user with threshold values. At this stage, membership in each set of fractures is determined based on the normal vectors of each point that constitute the fractures. Afterward, a final normal vector is fitted to each obtained cluster, modeling the fracture surface of the digitally acquired outcrop (clustering process of SEFL Module I, Fig. 1). The representativeness of the modeled fractures is also controlled by the real fracture size, roughness, HR-DTM point density, and scan accuracy (Jones *et al.*, 2015). Therefore, these clusters of points are used to characterize geometrical properties such as centroid position, orientation, and clustered points. The duration of this computing process is entirely dependent on the size of the point cloud, but it is the most time-consuming step of the workflow.
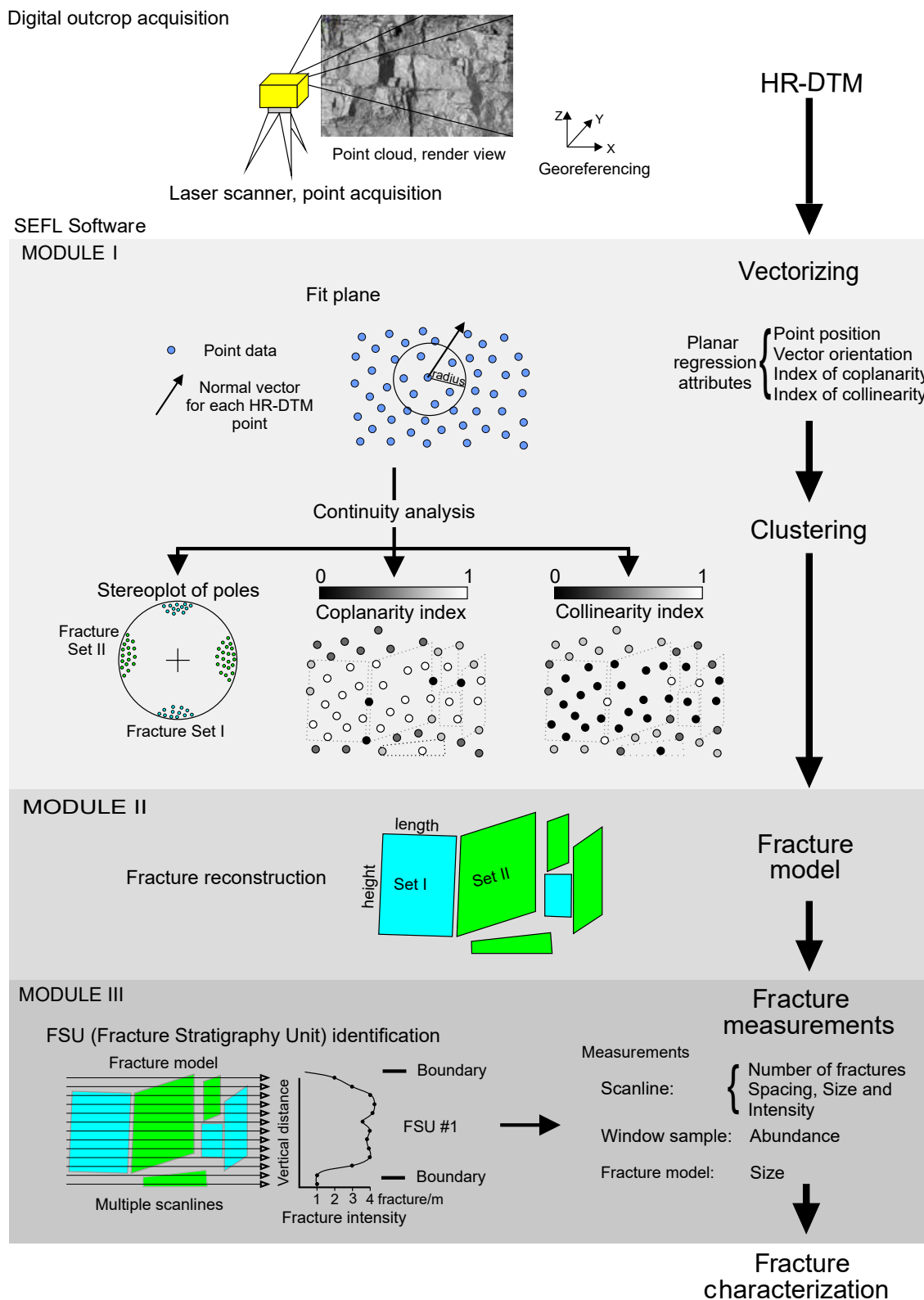
FIGURE 1. Workflow depicting the different modules of SEFL software for rock mass fracture characterization, after a previous acquisition to obtain an HR-DTM. Module I vectorizes the point cloud to determine planar regression attributes. Module II reconstructs fractures from point cloud clusters defining the fracture model. Module III analyses the fracture model to compute fracture intensities and contribute to determining the boundaries of each fracture stratigraphy unit.

Fracture modeling (SEFL Module II)

SEFL Module II implements algorithms to select the final cluster points and reconstructs fracture planes (fracture model process of Module II, Fig. 1) (Santana *et al.*, 2012). The complete set of reconstructed outcropping fractures constitutes a fracture model, with each fracture having associated geometrical properties of height and length (in a rectangular approach) while preserving the attributes of position and orientation. The complexity of this module lies in defining the parameters to obtain an optimal fracture model. The time required for this process is more dependent on the outcrop than on the processing time on a standard computer.

Fracture Stratigraphy Unit identification (SEFL Module III)

SEFL Module III is dedicated to identifying the boundaries of each FSU to characterize the fracture system by units (fracture measurement process of Module III, Fig. 1). For this purpose, the method implemented in SEFL Module III uses fracture intensity (number of fractures per survey length) as an attribute to identify FSUs (Fig. 1). The algorithm counts fractures from the fracture model that intersect with a plane drawn by the user, such as bedding or any reference plane (Massiot *et al.*, 2017). This process is analogous to the scanline counting method used in the field, where the first and last fractures intersected along the scanline mark its length. This counting is repeated using multiple scanlines that survey the entire fracture model at regular intervals defined by the user, always parallel to the referent plane.

The resulting number of fractures per meter for each scanline is integrated into a single graph along the height of the stratigraphic sequence or rock mass surveyed (Module III, Fig. 1) (Bertotti *et al.*, 2007; Hardebol and Bertotti, 2013). Afterward, this graph requires user analysis to identify significant changes in fracture intensity that are interpreted as the boundaries of each FSU. This process is empirical and necessitates subjective interpretation to mark boundaries and decide which layers belong to each unit. Consequently, the boundaries and thicknesses of each FSU are established.

In the second stage, SEFL Module III locates the centroid of each fracture within the fracture model and assigns it to the respective FSU. The properties of each fracture are associated with its centroid, enabling the calculation of parameters that characterize the fracture network by fracture set and FSU (fracture characterization process of Module III, Fig. 1).

Fracture Characterization (SEFL Module III)

SEFL Module III computes the parameters of the geometric characterization after identifying the boundaries of each mechanical unit (fracture measurement process of Module III, Fig. 1). This process locates each fracture centroid within its mechanical unit to survey and characterize the fractures network in a second stage. This characterization is fed with the attributes associated with the fracture model, selected either on the scanlines or contained within the sampling window (fracture characterization process of Module III, Fig. 1). Calculation times do not exceed a few minutes once the parameters that control each stage are established.

Fracture parameters

The main properties that characterize fractures within a fracture network are described below. This description includes a brief comparison between classical field data collection methods and the measurements obtained from the fracture model generated previously in our workflow.

i) Fracture orientation: This property is measured with the representation of the fracture surface on a plane. In the field, it is measured with a compass and the data can be discomposed into two components: azimuth (horizontal angle from the North) and dip (vertical angle). SEFL Module I fits a plane from the selected points representing a fracture surface and calculates the normal vector to derive the orientation, using the dip direction and dip convention.

ii) Fracture position: In the field, the position of a fracture is determined by the intersection between the fracture and the tape along a scanline. In SEFL Module I, the tool calculates the center of mass of the cluster of points intersected by the scanline plane, employing the eigenvector to represent the fracture surface position.

iii) Fracture size: Usually, fractures do not outcrop displaying all their dimensions due to censuring or truncation effects. The visible dimensions are typically measured with two parameters: length (parallel to the reference surface) and height (perpendicular to the reference surface). Algorithms in SEFL Module II obtain both parameters from the fracture model, computed according to the fracture orientation, and measured their maximum extension in relation to the reference orientation. Results are reported as mean values and cumulative frequency distribution graphs.

iv) Fracture aperture: This is the width of the space between both surfaces of a fracture. Mesoscale fractures have apertures ranging from millimetric to centimetric scale, which are visible and measurable in the field or in boreholes with a tape. Due to the insufficient resolution of the HR-DTM, apertures within this range must also be measured in the field.

Additional qualitative information, such as fracture aperture, the nature of the infilling materials within the fractures, fracture termination types, displacement indicators (*e.g.* slickenlines) or topology (Priest, 1993) must be also collected in the field and later, introduced into SEFL software to calculate porosities.

Fracture set parameters

Fractures are grouped by similar properties, mainly their orientations and type, as observed statistically by the user and the relationships between different fracture surfaces in the field or within the fracture model. Consequently, various thresholds are established to determine each set of fractures. SEFL Module III simulates the field scanline measures by projecting a plane, through the center of the FSU, parallel to the boundary of the unit, which intersects with the fractures of the fracture model. These intersections are used to calculate the following parameters for each fracture set and where it is possible to present the characterization by mechanical unit (Priest, 1993):

i) Number of fractures: This is the count of fractures intersected along each scanline.

ii) Mean orientation of the intersected fractures: This is calculated using the vector direction methodology (Fisher, 1985) for populations with a single polarity.

iii) Fracture spacing: This is the distance between two adjacent fractures of the same fracture set, measured along the perpendicular-to-fracture vector (Gross, 1993; Narr and Suppe, 1991; Terzaghi, 1965). Field measurements require trigonometric corrections to convert the apparent spacing between two adjacent fractures into real spacing (Terzaghi, 1965). In SEFL Module III, spacing is measured from the centroids of the two adjacent fractures of the same fracture set along the normal vector of the first fracture.

iv) Fracture spacing is typically characterized by its mean value, standard deviation, standard deviation ratio (standard deviation divided by the mean), Coefficient of variation (Cv) (Gillespie *et al.*, 1999) or ratio of standard deviation (standard deviation divided by mean space) and cumulative distribution graph. The standard deviation reports the type of dispersion of the fracture spacing values compared to the mean while the coefficient of variation indicates whether fracture distribution is clustered or not. Cv values close to 0 indicate regularly distributed fractures, values close to 1 indicate a random distribution, and values greater than 1 indicate that fractures are clustered.

v) Vertical persistence: This quantifies the proportion of fractures crossing a mechanical layer boundary along the scanline (Bech *et al.*, 2001; Gillespie *et al.*, 2001; Petit *et al.*, 1994). In SEFL Module III, vertical persistence is calculated using the fracture model properties of position and height with respect to the FSU thickness. Fractures contained within a single layer are referred to as strata-bound (Odling *et al.*, 1999). Conversely, fractures not constrained by their single layer boundaries are considered non-strata-bound.

vi) Fracture spacing ratio and index (Gross, 1993; Narr and Suppe, 1991). These indices are employed to normalize fracture spacing according to mechanical layer thickness and are used in cases where fractures are confined within their mechanical layer. The fracture spacing ratio is the ratio between the mechanical layer thickness and the median fracture spacing. The fracture spacing index is the slope of the linear regression between the mechanical layer thickness and the median fracture spacing (Narr and Suppe, 1991).

vii) Fracture abundance: This describes fracture systems in terms of the amount of fracturing through measures of fracture density, intensity, and porosity (Dershowitz and Herda, 1992; Mauldon, 1994). Measures are referred to in the P_{xy} system, where x is the sampling domain (linear, areal, and volumetric) and y is the feature measured (number, length, area, and volume of the fractures). Fracture density describes the number of fractures per length (P_{10} or linear density), per area (P_{20} or trace density), or per volume (P_{30} or volumetric density). Fracture intensity describes the height of fracture traces per area of exposure (P_{21}) and volumetric intensity is the area of fractures (height by length fracture) per volume (P_{32}). SEFL Module III adopts the P_{1y} counts by applying the scanline method by projecting a plane in the middle part of the mechanical layers, while the P_{2y} values are measured using the window sample method between the limits of each FSU.

viii) Fracture porosity: This parameter requires aperture values of the fractures to define linear porosity (P_{11}), areal porosity (P_{22}), and volume porosity (fracture porosity) (P_{33}). It is worth mentioning that the volumetric parameters P_{32} and P_{33} cannot be determined directly from the outcrop surface. To amend this, Wang (2005) proposed inferring them with linear intensity (P_{10}) and areal intensity (P_{21}) and quantifying volumetric intensity (P_{32}) and fracture porosity (P_{33}) via Equations (1) and (2) with the conversion factor C, where α is the angle between the sampling line and the normal vector of the fracture, β is the angle between the normal vector of the sampling plane and the normal vector of the fracture, $fA(\alpha)$ and $fB(\beta)$ are the probability distribution function of the angles α and β.

Eq. 1: $P_{32} = P_{10} \int_0^\pi cos\alpha \vee fA(\alpha)d\alpha = P_{10}C_{13}$

Eq. 2: $P_{32} = P_{21} \int_0^\pi sin\beta fB(\beta)d\beta = P_{21}C_{23}$

ix) Fractal dimension: The property analysis of fractures and fracture sets is generally supported by statistical representation of data sets, such as histograms and cumulative distribution graphs (Bonnet *et al.*, 2001). These values are typically fitted to an exponential, logarithm, gamma, normal, or power law distribution, simplifying the representation of the property and enabling projections at scales where they have not been sampled (Bonnet *et al.*, 2001; Gillespie *et al.*, 1993). Additionally, a cumulative distribution function may be used to determine the fractal dimension when a power law distribution is fitted across multiple orders of magnitude (Gillespie *et al.*, 1999; Mandelbrot, 1982).

APPLICATION: THE AÑISCLO ANTICLINE CASE STUDY

Geological Setting

The Añisclo, Mediano, Olsón and Boltaña anticlines are part of the Sobrarbe fold system in the Ainsa fold and thrust oblique zone of the Central Pyrenees (Fig. 2A; Fernández *et al.*, 2012; Muñoz *et al.*, 2013). These north-south trending anticlines are over 10km long and have at least 1000 meters of structural relief. They developed during the Pyrenean Orogeny along the eastern margin of the Gabarnie-Sierras Exteriores thrust sheet, in the footwall of the Montsec-Peña Montañesa and the Monte Perdido thrust sheets (Fernández *et al.*, 2012; Tavani *et al.*, 2006).

Structural, sedimentological and paleomagnetic data from the Sobrarbe fold system reveal that this set of N-S anticlines experienced a clockwise vertical axis rotation synchronous to their growth (Muñoz *et al.*, 2013). In this sense, the Añisclo anticline originally formed with an E-W trend that progressively rotated to the present-day N-S attitude (Fernández *et al.*, 2004; Muñoz, 2017; Muñoz *et al.*, 2013; Tavani *et al.*, 2006). This progressive rotation occurred simultaneously to the divergent thrust transport trajectories constrained by the Upper Triassic salt basin distribution resulting in the development of a thrust salient in the Southern Pyrenees (Muñoz *et al.*, 2013).

The Añisclo anticline plunges 10º southwards in its central part, where it corresponds to an asymmetric fault propagation fold with a vertical to steeply overturned western frontal limb that progressively opens southwards into an anticline detached along Upper Triassic evaporites with a plunge of 25º (Figs. 2B; 3; Fernández *et al.*, 2012; Muñoz *et al.*, 2013; Tavani *et al.*, 2006). These evaporites are overlaid by Upper Cretaceous marls and limestones cropping out in the core of the Añisclo anticline (Fig. 2B). Paleogene rocks, characterized by Paleocene to the middle Eocene limestones and marls are unconformably overlain

by middle Eocene (Lutetian) turbidites of the Ainsa system corresponding to the oldest growth strata sediments (syn-folding rocks) (Fig. 3; Arbués *et al.*, 2007; Muñoz *et al.*, 2013).

Outcrop characteristics and data acquisition

Fracture characterization was conducted using the presented methodology for a selected outcrop. This outcrop is partially located at the hinge of the anticline and at the eastern limb, and includes marly limestones intercalated with clay layers of the Eocene Metils Formation (Fm.) and at the mesoscale presents the structure of a fracture system (Figs. 2 to 4). The Metils Fm. comprises a 10m-thick basal interval of marly micritic limestone interbedded with 20cm-thick silty layers. At the upper part of the Fm., the limestones are interbedded with 30cm-thick marl layers (Rios *et al.*, 1979). According to Van Lunsen (1970) and Rios *et al.* (1979) the fossiliferous content of this Fm. includes *Globorotalia gracilis-formosa*, *Globigerina (Acarinina)* aff. *mckannai*, *Globigerina* aff. *gravelli*, *Globigerina* aff. *soldadoensis* thus confirming its Eocene age. Along the 220m-long and up to 8m-high outcrop, with mean bedding thickness of around 30cm, more than forty bedding surfaces were identified. Many of these surfaces are discontinuous laterally and beds appear massive, resulting in an alternation of thin and more massive layers (Fig. 4). This distribution complicates the identification of the stratigraphic and mechanical layer boundaries along the entire outcrop. The mean bedding dip is 141/28 (dip direction convention) with a stratigraphic thickness of 18.37meters.

Ten TLS stations (model Optech ILRIS-3D equipped with Differential Global Positioning System) were utilized to acquire 41 laser images of the outcrop to complete a georeferenced HR-DTM of 24.5 million points (Fig. 4). The HR-DTM model was divided into two sectors according to the outcrop face orientation: NE-SW and N-S (Fig. 4A, B, D). Moreover, the field survey was supplemented by five manual scanlines parallel to the bedding and 20 Schmidt hammer rebound tests to analyze the mechanical behavior.

Results: Fracture surface characterization

The fracture model produced using SEFL software contains 669 fractures in the NE-SW sector and 1119 fractures in the N-S sector (Fig. 4C, E), while 121 fractures were identified and measured directly using the conventional manual scanline method.

Fractures modeled with SEFL software and classical scanlines were plotted as poles to fractures and cumulative contouring equal-area stereoplots (Fig. 5) and have been classified into five fracture sets. For instance, the boundary
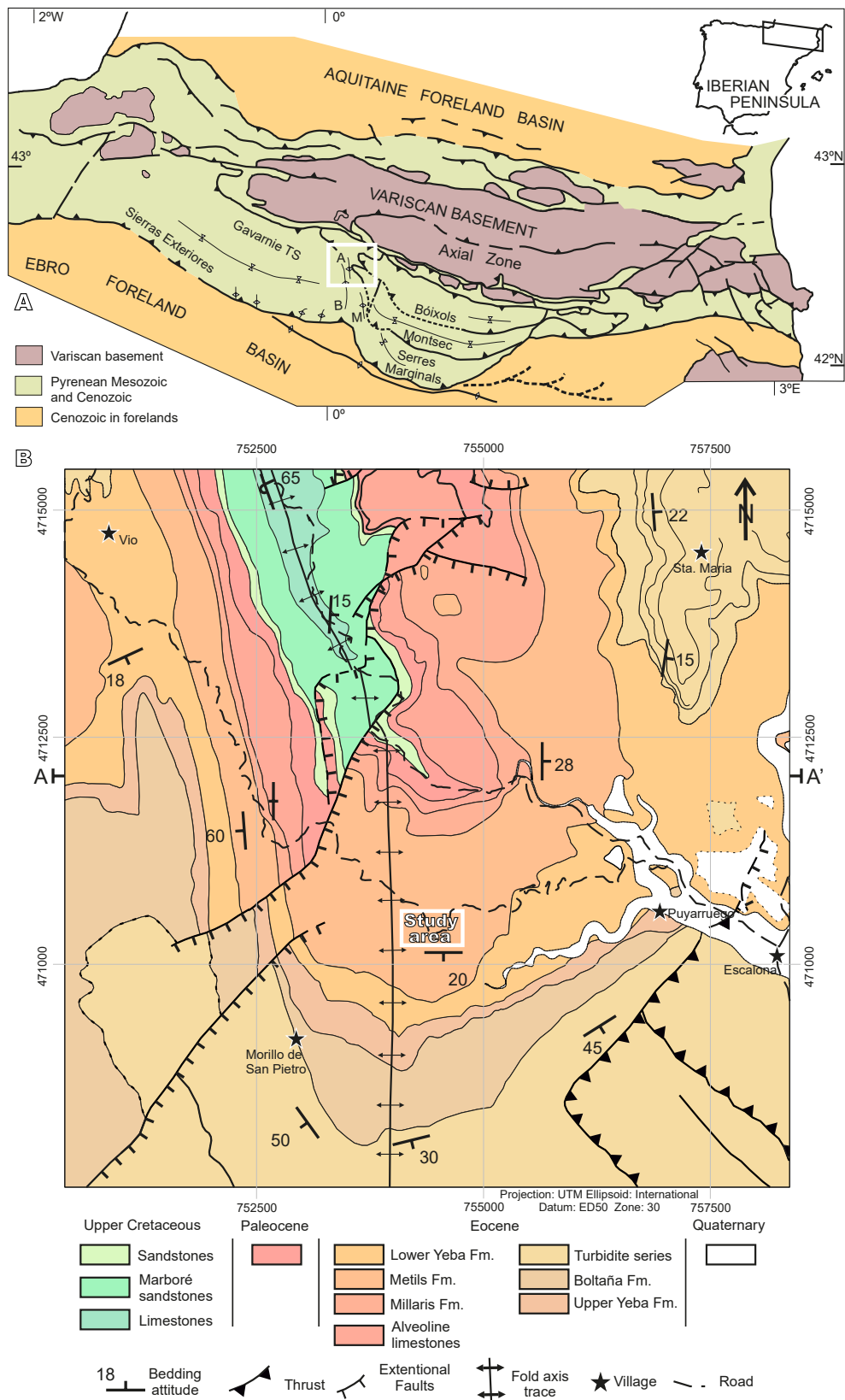
FIGURE 2. A) Structural map illustrating the main structural units of the Central Pyrenees. The white box indicates the location of the detailed Añisclo anticline geological map. A: Añisclo anticline, B: Boltaña anticline and M: Mediano anticline. B) Detailed geological map of the Añisclo anticline, showing the location of the studied outcrop (white box). A–A' corresponds to the detailed cross-section of the Añisclo anticline of Figure 3. Adapted from Mochales *et al.* (2012), Rios *et al.* (1979), Robador and Zamorano (1991) and Tavani *et al.* (2006).
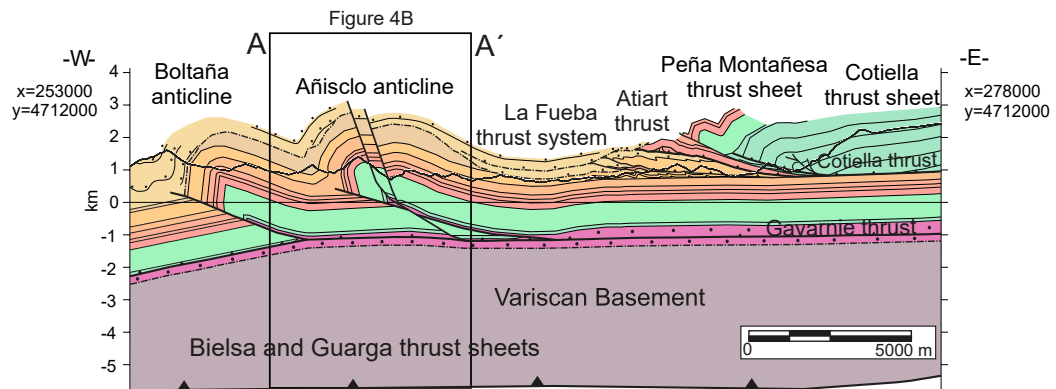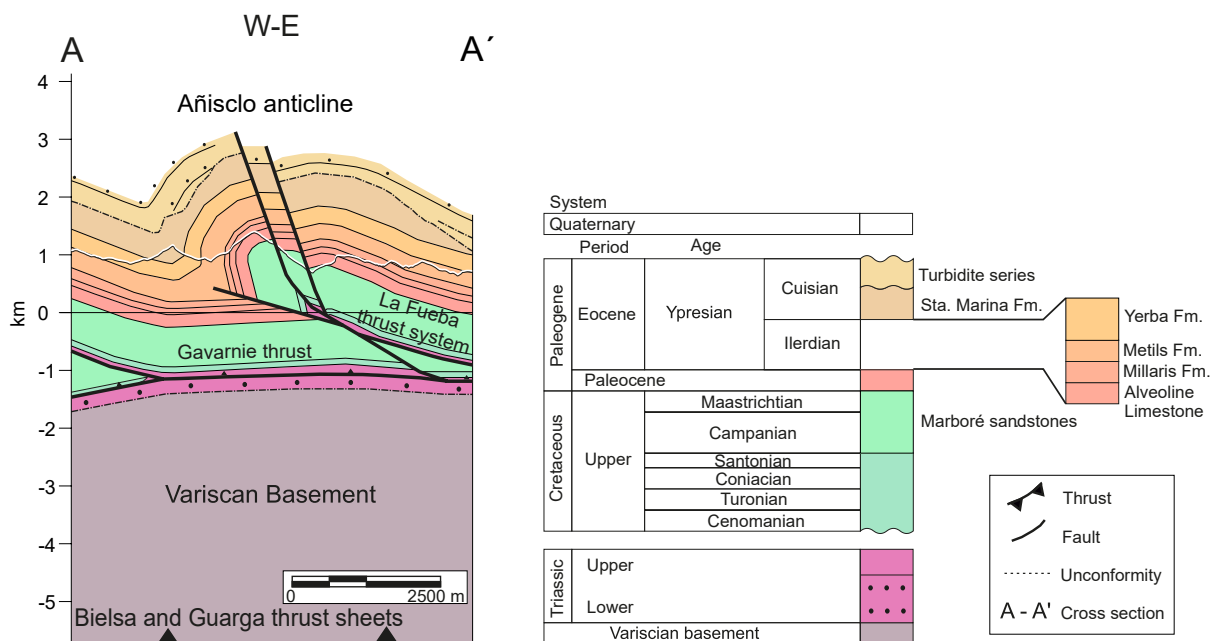
FIGURE 3. A) General cross-section of the area. B) Detailed cross-section centered on the Añisclo anticline (location shown in Fig. 2). Adapted from Muñoz *et al.* (2013).

between Fracture Sets III and IV is clearly distinguishable in the field, with fractures intersecting each other.

The subdivision into mechanical units, based on visual analysis of SEFL Module III fracture intensity graph and significant lithological variations, reported 14FSUs (Fig. 6). Multiple scanlines were spaced at 10cm intervals along the stratigraphic thickness (18.37m) to capture detailed variations in fracture intensity. Additionally, the Schmidt hammer rebound test revealed differences in compressive strength along the outcrop profile (Fig. 6).

In the N-S sector, the greatest number of fractures belongs to Fracture Sets V and I (350 and 332 fractures, respectively), followed by Fracture Set III (221 fractures), Fracture Set IV (126 fractures), and Fracture Set II (90). In the NE-SW sector, Fracture Set III (242 fractures) and Fracture Set IV (212 fractures) are the most numerous, followed by Fracture Set I (130). Fracture Sets V and II are the less frequent with 49 and 21 fractures, respectively.

The fold axis in the study area generally trends N-S (Fig. 3) with a slight westward component. Fractures in Fracture Set V are parallel to the fold-axis, while fractures in Fracture Set III are oblique to it.
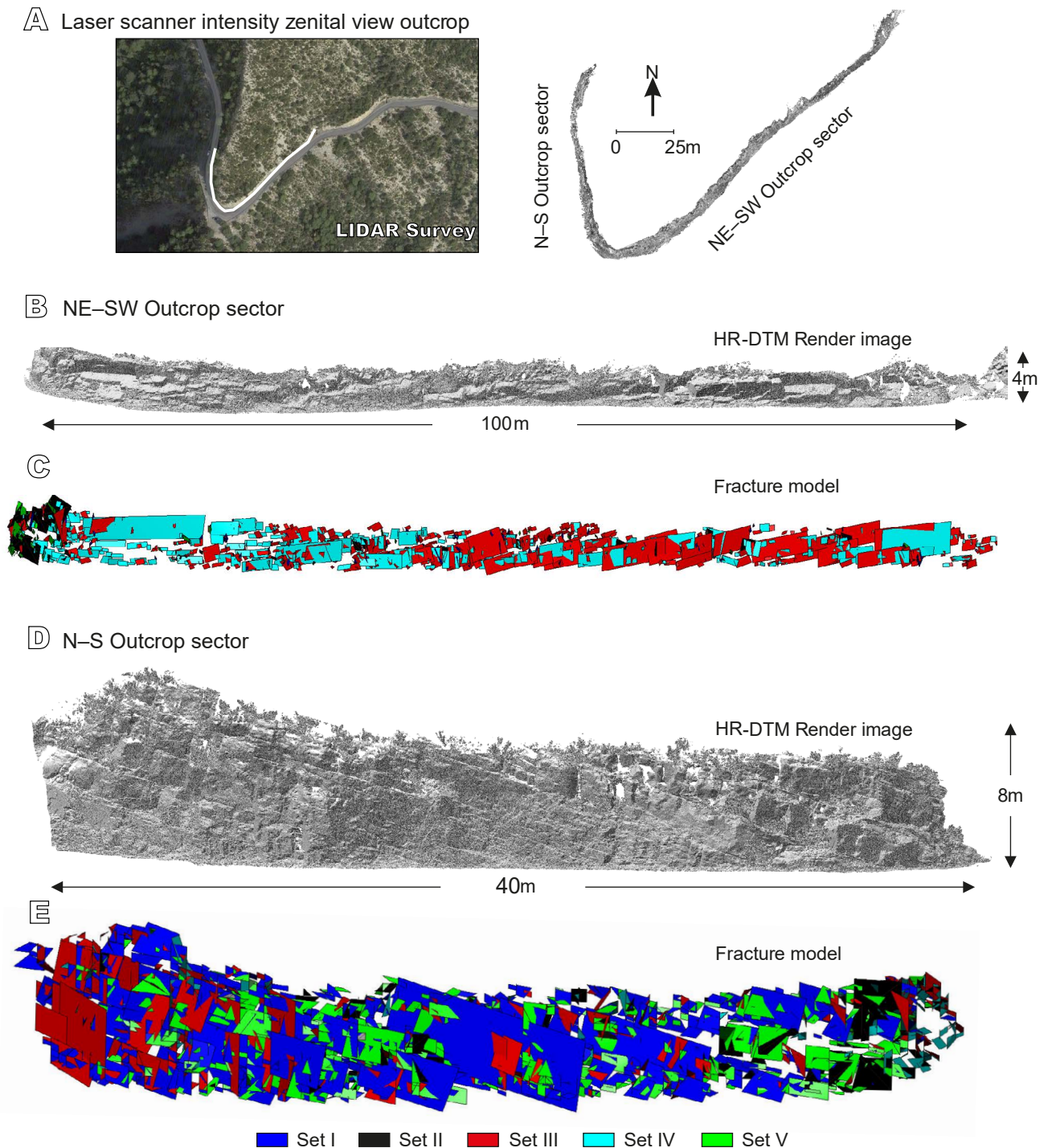
FIGURE 4. HR-DTM and the fracture model. A) Plan view of the HR-DTM showing the N-S and NE-SW oriented outcrop sectors. B) Render view of the NE-SW sector HR-DTM. C) NE-SW sector fracture model. D) Render view of the N-S sector HR-DTM. E) N-S sector fracture model.

The number of fractures intersected by each scanline measured in each FSU processed by SEFL Module III, range from 15 to 75, with scanline lengths between 10 and 40m (Fig. 7A). The five manual scanlines intersected fewer fractures (approximately 25 per scanline) with shorter lengths (less than 30m). Both sectors (NE-SW and N-S) show differences regarding the dominant fracture sets (III, IV and V), though a significant number of fractures from Fracture Set I are also notable. The fracture intensity, normalized by scanline length, ranges from 1.5 to 3.376 fractures/m for both sectors, with slightly lower values for manual scanlines (Fig. 7B).
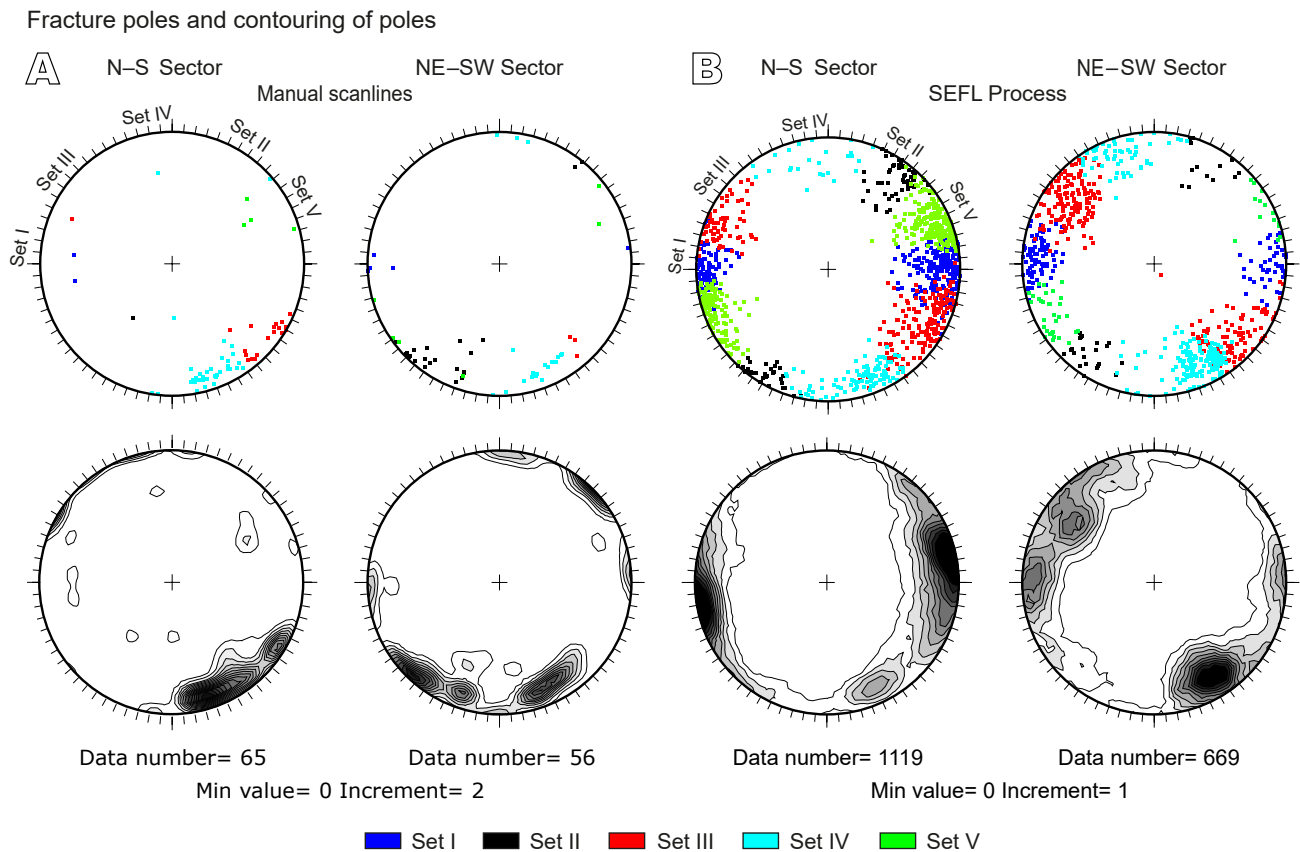
FIGURE 5. Stereographic projection (upper images: equal-area lower hemisphere stereoplots) of fracture orientation poles and the corresponding contouring of total fracture poles (lower images). A) Fractures measured directly at the outcrop using a compass during manual scanlines. B) Fracture orientation calculated from the SEFL fracture model for the N-S and the NE-SW sectors. Poles are colored by fracture set. Stereoplot projections were generated using Open Plot software by Tavani *et al.* (2011).

Fracture spacing values vary, from decimetric distances for the most abundant fracture sets to metric values for the remaining fracture sets (Fig. 7C). Coefficients of variation for the entire outcrop are mainly clustered between 0.5 and 2 (Fig. 7D). Fracture spacing exhibits a power law distribution in both sectors with acceptable quadratic fit errors to the curvatures described for each fracture set (Fig. 8).

Typically, the mean heights of fractures surveyed with SEFL are less than 1.5m without crossing the FSU boundaries (Fig. 9A). Exceptions include thinner FSUs 11-14 and Fracture Sets I and IV, which have mean heights of up to 2.5m, reflected in the low proportion of fractures exceeding FSU boundaries (Fig. 9B). The mean fracture length is shorter than one meter for most FSUs with a few exceptions (Fig. 9C). The height cumulative distribution graph for the total fracture model shows a good fit with exponential functions for each fracture set (Fig. 10A), with the best-fits between heights of 0.2m and 1.5-3m, losing accuracy with less frequent heights. The cumulative distribution graph for fracture length shows the best-fit for power law functions between lengths of 0.2m and 3m (Fig. 10B).

Abundance results, measured using the window sample process in SEFL Module III, show a similar number of fractures in areal density (P_{20}) for both sectors, less than 2-3fractures/m^2, except for FSU 14. The majority of FSUs in the N-S sector have densities below 2fractures/m^2, while some FSUs in the NE-SW sector reach up to 4, 7 and 14 meters by trace length per m^2 (Fig. 11A, B).

Volumetric intensities ($P_{32}(C_{13}P_{10})$) calculated from linear intensity (P_{10}) vary between 0.5 and 2.5m^2/m^3 in the N-S sector and between 1 and 4m^2/m^3 in the NE-SW sector (Fig. 12A). Volumetric intensities ($P_{32}(C_{23}P_{21})$), calculated from the areal intensity value (P_{21}), show similar ranges, between 2 to 5m^2/m^3 for both sectors for the dominant fracture sets (Fig. 12B). Volumetric intensities ($P_{32}(C_{13}P_{10})$) calculated with manual scanlines data, present irregular and higher values than the values from SEFL software (Fig. 12A). Fracture apertures measured at the outcrop show a
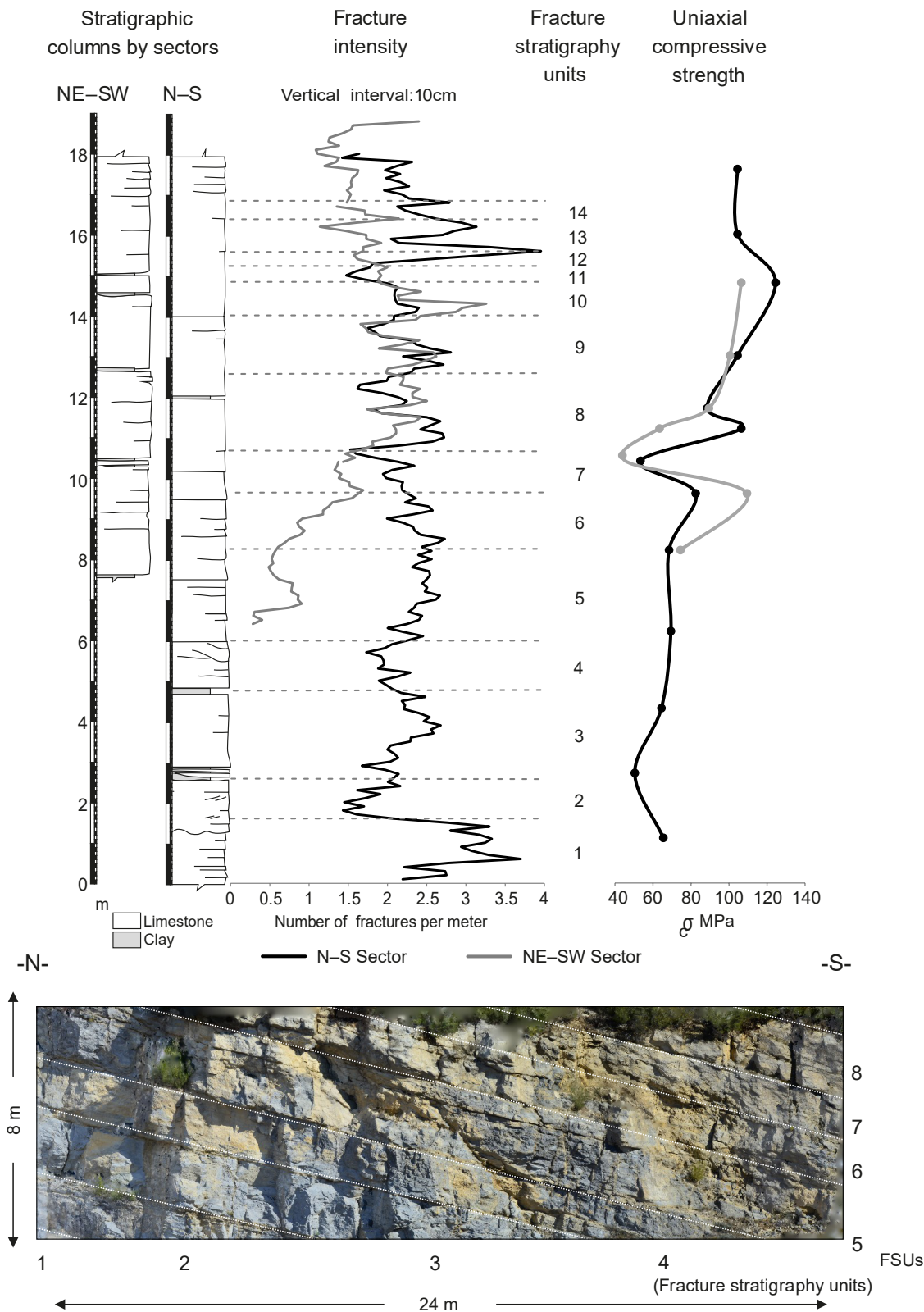
FIGURE 6. FSUs identification methodology based on fracture intensity, and two stratigraphic representative stratigraphic columns of the outcrop and Schmidt hammer rebound test values for both sectors of the studied outcrop (black line: N-S; grey line: NE-SW sector). Fourteen FSU were determined to characterize mechanically the outcrop. The correlation for calculating the Uniaxial Compressive Strength values was derived using the chart developed by Miller (1965), with a density value for limestone at 2.65g/cm³ after filtering extreme values from the set of 10 rebound. The standard test method followed American Society for Testing and Materials (2005) recommendations.
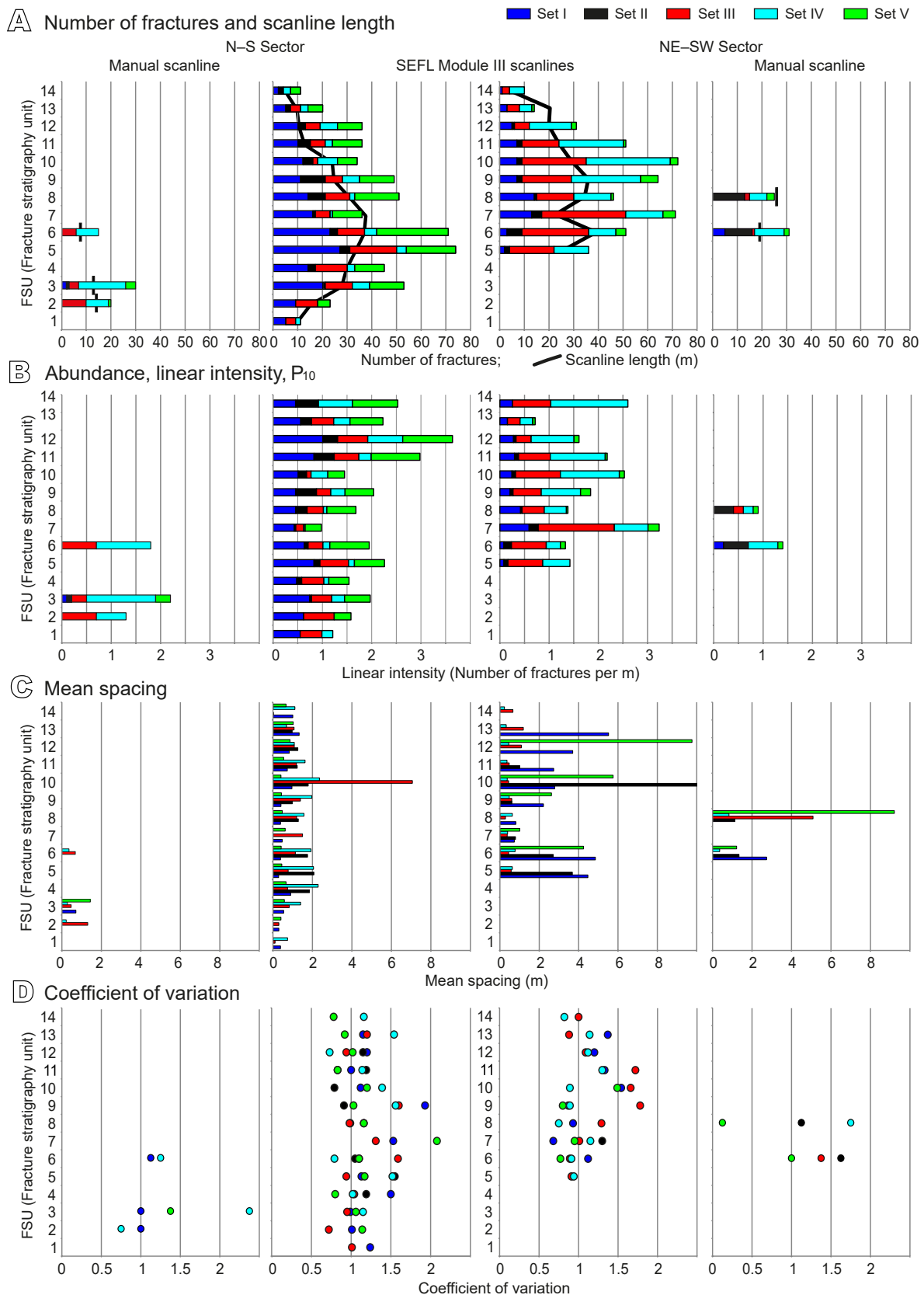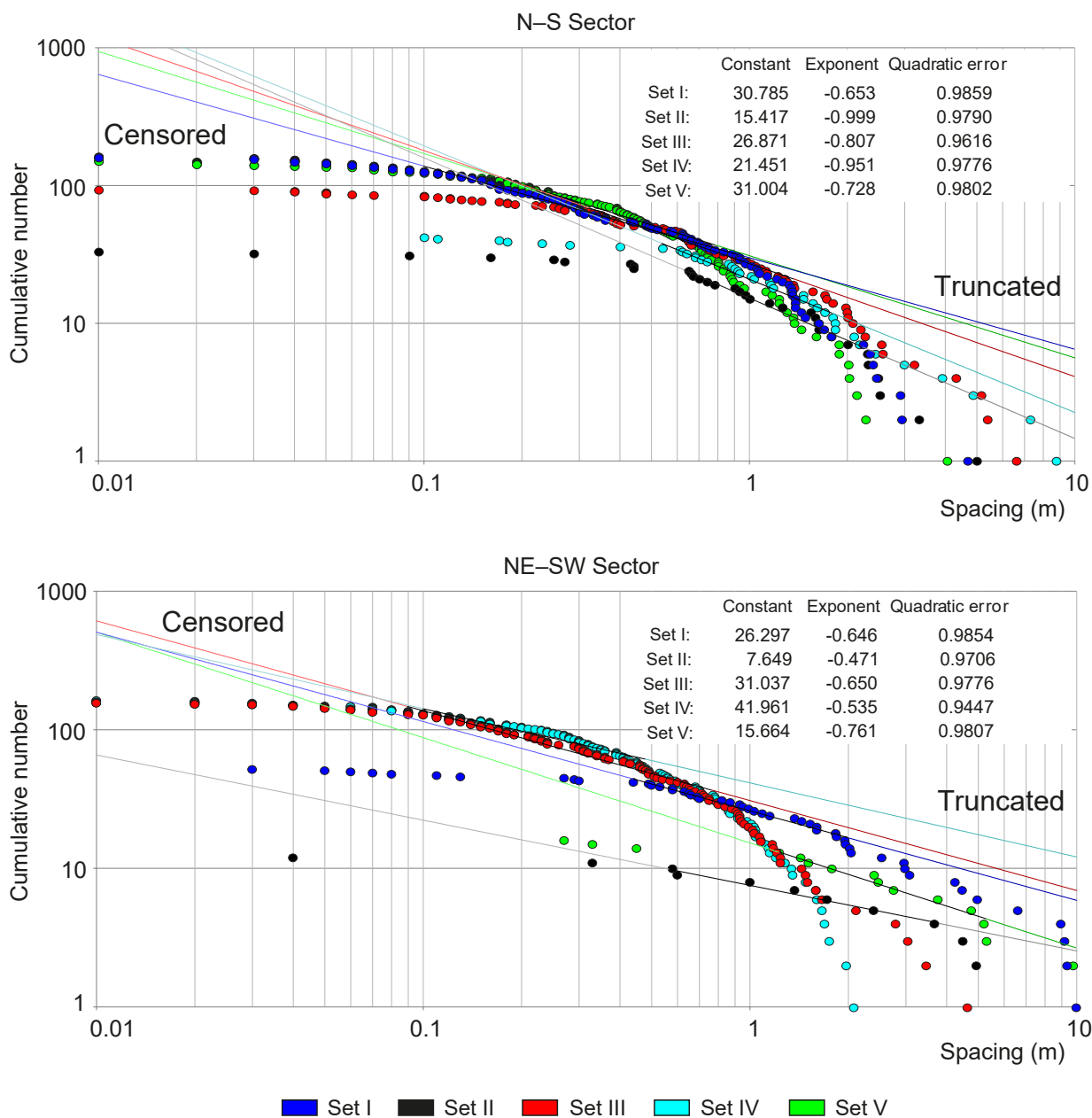
FIGURE 7. Parameters measured and calculated with the manual and SEFL samples plotted for each FSU, outcrop sector and fracture sets (bar chart). A) Number of fractures and the length of the scanlines (black line chart). B) Fracture linear intensity (P_{10}). C) Mean fracture spacing. D) Coefficient of variation.

Cumulative frequency spacing

FIGURE 8. Spacing values of the different fracture sets for each outcrop sector. A power-law function was fitted to each fracture set data, and statistical results of the power-law function fit are included.

wide range of values, from 0.2 to 5mm, filled with calcite (Fig. 13).

DISCUSSION

This section is divided into two subsections. The first subsection tackles the methodology presented in this work while the second is focused on the Añisclo case study.

Data processing with SEFL software

Manual fracture digitalization in a 2D/3D environment (using images, HR-DTM or point clouds) is a solvent methodology supported by the interpretation of the user to develop fracture models (Assali *et al.*, 2014; Bertotti *et al.*, 2007; Geyer *et al.*, 2015; Gigli and Casagli, 2011; Hardebol and Bertotti, 2013; Hodgetts *et al.*, 2007; Seers and Hodgetts, 2014; Tavani *et al.*, 2014). The disadvantage

## Ⓐ Fracture mean height and FSU thickness
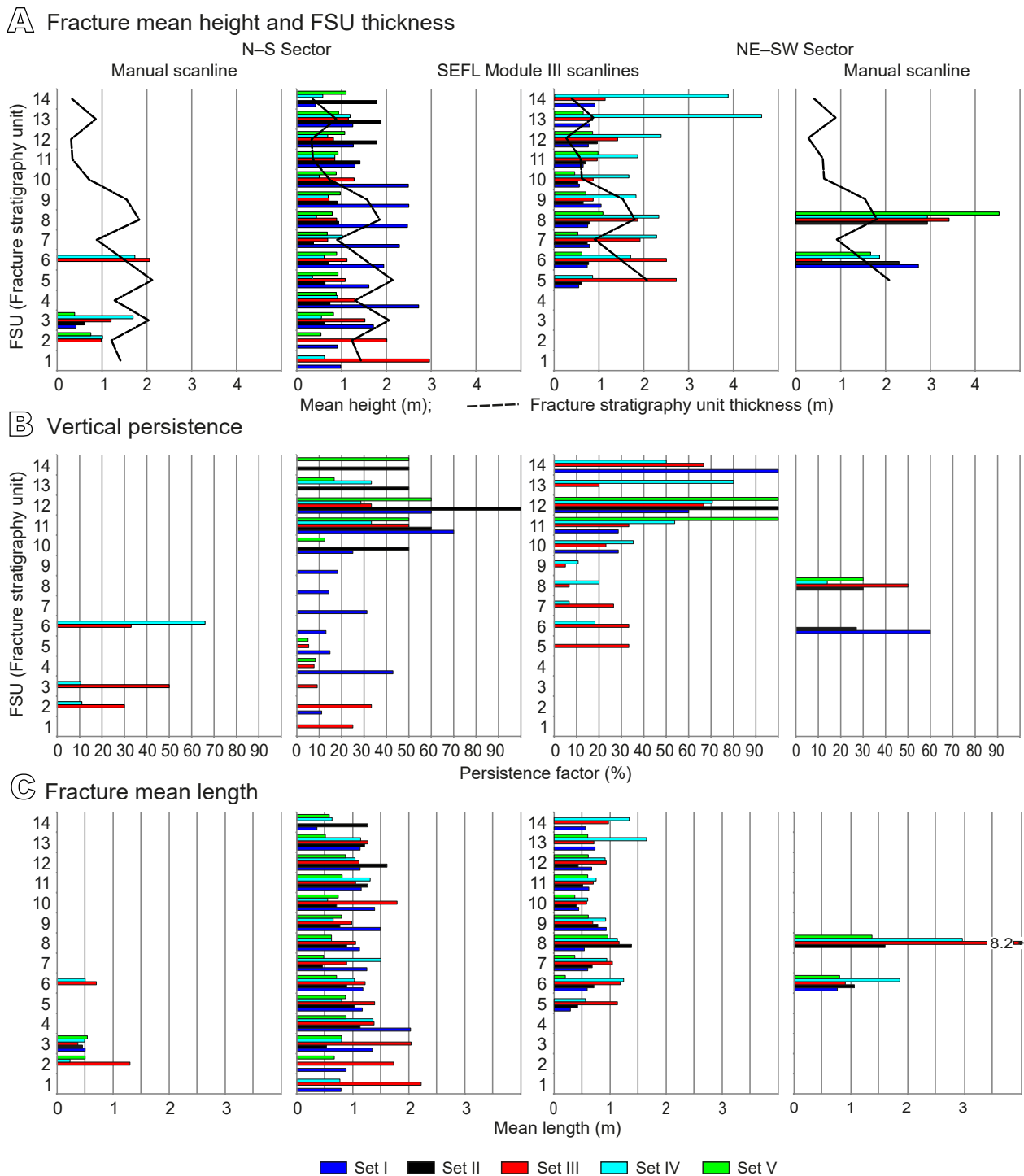
FIGURE 9. Fracture parameters measured and calculated with manual and SEFL scanlines for each FSU and by fracture set with Module III. A) Mean fracture height (bar chart) and FSU thickness (discontinuous line chart). B) Vertical persistence shows the fraction of fractures that exceed the bounds of each FSU. C) Mean fracture length.

of this approach resides in the considerable time required to identify and digitalize the fracture system. On the other hand, automatic identification of fracture surfaces has a better aptitude for managing a large number of fractures and a lesser ability for fracture identification (Garcia-Sellés

et al., 2018; Jaboyedoff *et al.*, 2007; Lato and Vöge, 2012; Massiot *et al.*, 2017; Olariu *et al.*, 2008; Slob *et al.*, 2005). Regardless of the methodology used to achieve a fracture model, SEFL Module III is a tool intended to compute statistical fracture properties.
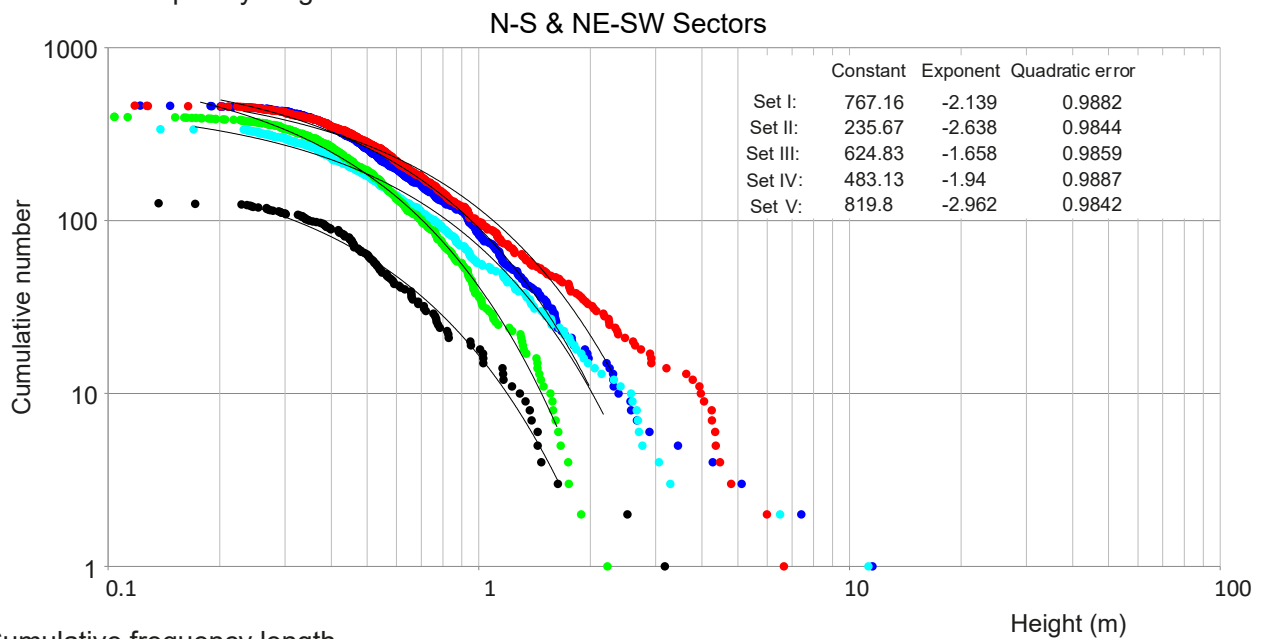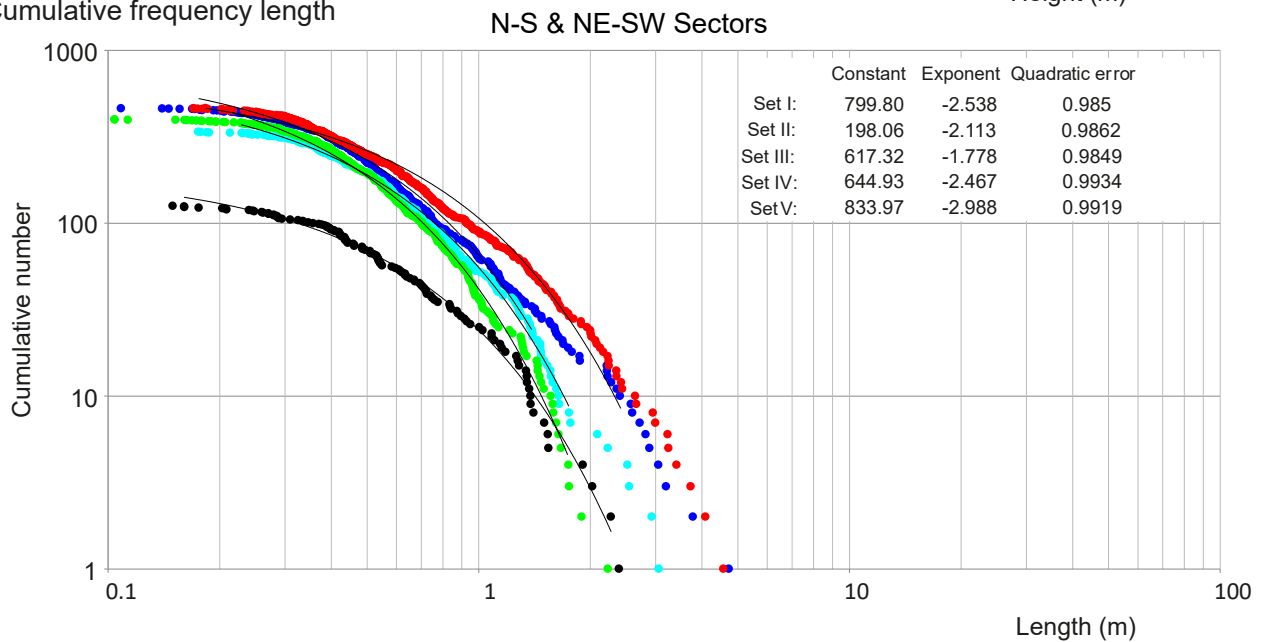
FIGURE 10. Size fracture properties, height and length, from the SEFL fracture model for the fracture sets. A) Cumulative distribution of fracture height. B) Cumulative distribution fracture length. Each fracture set was fitted with a power law function, and statistical results of the power law function fits are included.

SEFL Modules I and II, are essential preliminary steps for the subsequent fracture characterization in SEFL Module III. The accuracy of vectorizing and clustering HR-DTM data directly affects the fidelity of the fracture model, influencing the geometrical characterization and identification of the FSUs. Despite the automated nature of the methodology, significant time is required to configure parameters such as threshold values, distances, and boundaries. These parameters must be carefully determined by the user due to their impact on the results.

One limitation of the proposed methodology is its tendency to underrepresent the number and size of identified fractures, due to the challenges associated with
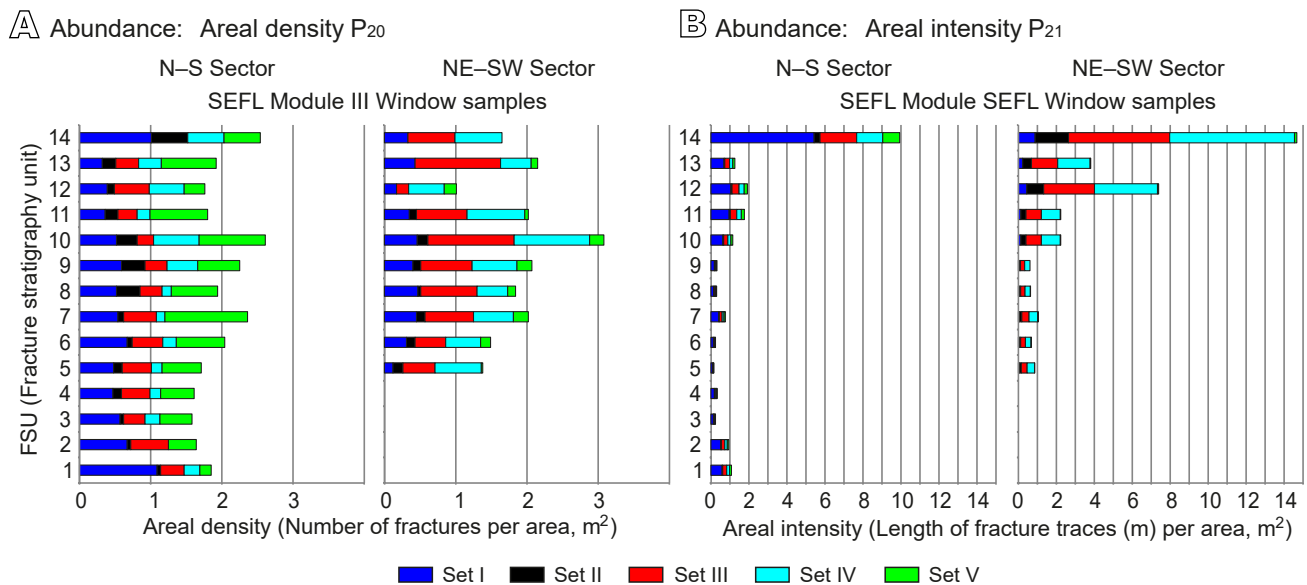
FIGURE 11. Areal parameters of abundance obtained from the SEFL fracture model. A) Areal density (P_{20}) and B) Areal intensity (P_{21}) calculated using the window sample method for each FSU and fracture set.

generalizing the definition of fracture to recognize it in an HR-DTM. Likewise, assigning fractures to their respective fracture sets based on the orientation of all their normal vectors generates uncertainties, as these orientations do not always align with the final orientation. This issue is illustrated in Figure 5, where some fractures do not precisely coincide with the boundaries of their fracture sets. Although there are many examples of TLS in the literature regarding fracture roughness (*e.g.* Mah *et al.*, 2013), the methodology in SEFL does not incorporate parameters such as aperture or roughness due to the lack of resolution in HR-DTM. Therefore, the aperture parameter has not been implemented and the porosity value is not determined. However, if this value is available from manual scanlines, the porosity parameter can be calculated in SEFL.

The characterization results are described where possible, using a deterministic or stochastic modeling for each fracture set and FSU, since this last approach is the most appropriated to define DFN models. The reliability of the results depends on the number of modeled fractures and the robustness of their statistics. Likewise, the use of remote sensors as the main source of data enables access to inaccessible or extensive areas where the scanline methodology cannot be feasibly applied.

Application in the Añisclo anticline

The fracture study conducted using the SEFL fracture model and classic scanlines identified five distinct fracture sets (Fig. 5). With regard to the mechanical behaviour of the massive rock in the outcrop, it is possible to affirm that

it is heterogeneous. It can be verified in both the result of the scanlines to determine the FSUs and the Uniaxial Compressive Strength values obtained from the Schmidt hammer rebound test (Fig. 6). Identifying the limits of the FSUs after data acquisition based on fracture intensity and the non-continuous lithological boundaries of the stratigraphic sequence, allowed for the study and selection among different solutions. While the boundaries of lithological layers were recognizable in certain sections, the boundaries of mechanical layers along the outcrop were not as discernible. The stratigraphic fracture solution provided additional information, although subjectively, to identify 14 mechanical units for sampling the characteristics of the fracture system.

The global intensities of these fractures ranged from 2 to 3 fractures per meter for each FSU and would mainly correspond to Fracture Set I. This set is considered one of the most dominant due to its high intensity values in the N-S sector (Fig. 7B). Both, the orientation and the fracture intensities are consistent with the previous study by Tavani *et al.* (2006) who reported the development of extensional structures during the evolution of Añisclo anticline.

The heterogeneity of the mechanical behavior is evident in the Uniaxial Compressive Strength recorded by the Schmidt hammer rebound tests and, in the scanlines, measuring fracture intensities to identify the FSUs (Fig. 6). However, it should be noted that the fracture intensity test reflects the conditions at the time of fracture development, unlike the Schmidt hammer rebound test.
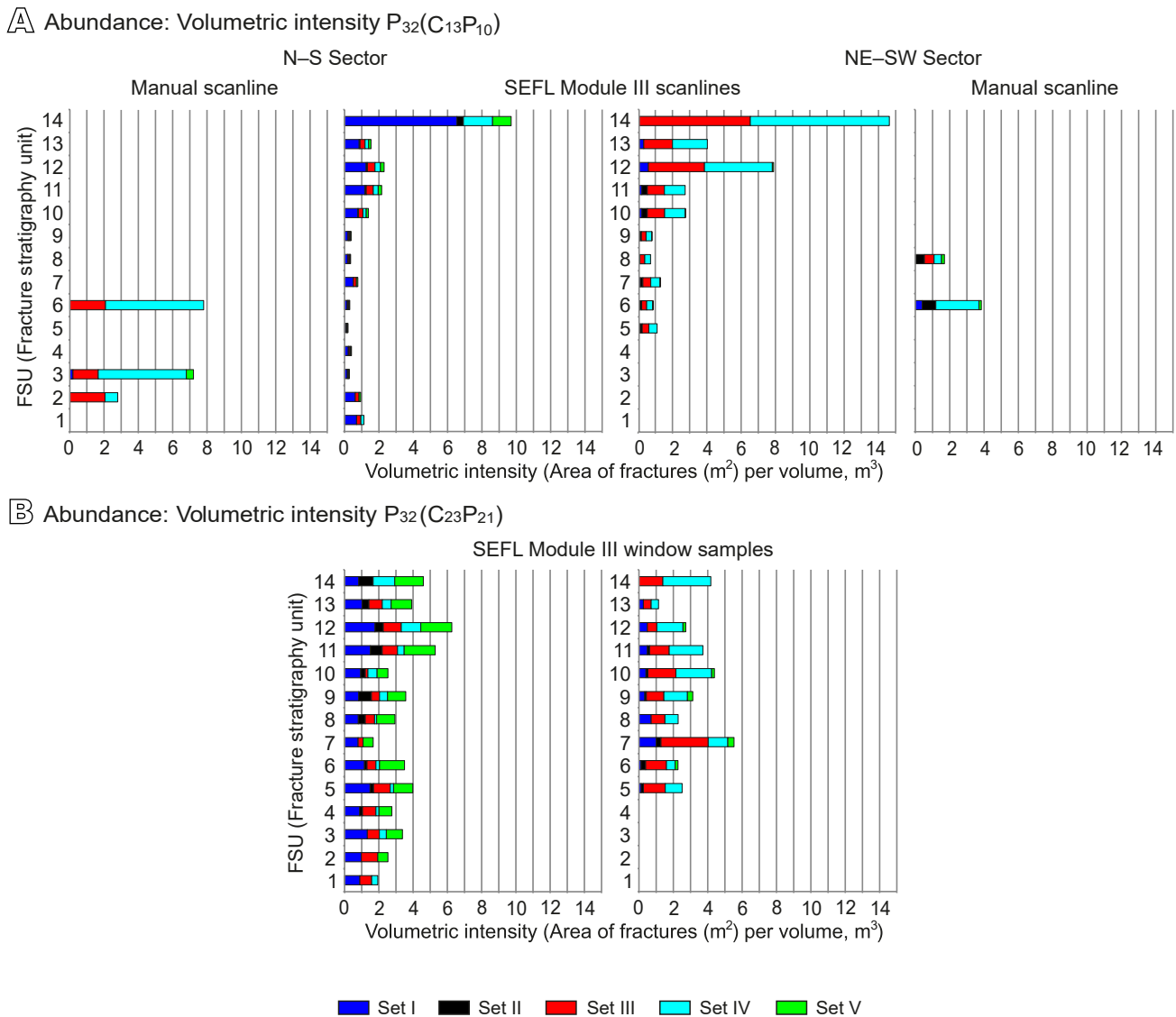
FIGURE 12. Volumetric parameters of abundance. A) Volumetric intensity calculated from the linear intensities ($P_{32}(C_{13}P_{10})$), available for both manual and SEFL process scanlines, and B) volumetric intensities, only available for SEFL scanlines ($P_{32}(C_{23}P_{21})$) for each FSU and fracture set.

Considering fracture heights and vertical persistence parameters, it is interpreted that the fractures are predominantly contained within the FSUs (Fig. 9A, B). Persistence values derived from manual scanlines are higher than those obtained through the SEFL process, due to the accuracy of the manual technique in identifying fracture tips. Generally, the fracture heights are below two meters and do not exceed the FSUs boundaries. This is corroborated by the cumulative distribution graph which displays low fitting errors in the power law function (Fig. 10A). Moreover, fractures identified as intact through manual scanlines, constitute about 40%, while those identified as not intact or obscured (*i.e.* fractures cropping out with incomplete length or without visible tips) reach

up to 50%, increasing the uncertainty of the real height of the fractures.

The N-S outcrop sector is characterized by the vertical fracture surfaces of Sets I and V with an orientation subparallel-to-outcrop (Fig. 4). Conversely, the NE-SW outcrop sector is morphologically conditioned by the parallel-to-strike nearly-horizontal apparent bedding attitude, facilitating the sliding of blocks bounded by the intersection of fractures and bedding. This relationship explains the better exposure of Fracture Set I lengths in the N-S sector compared to the NE-SW sector (Fig. 9C). Conversely, the fracture length exposure for Fracture Sets III and IV is better observed in the NE-SW sector. However,

Mean fracture aperture
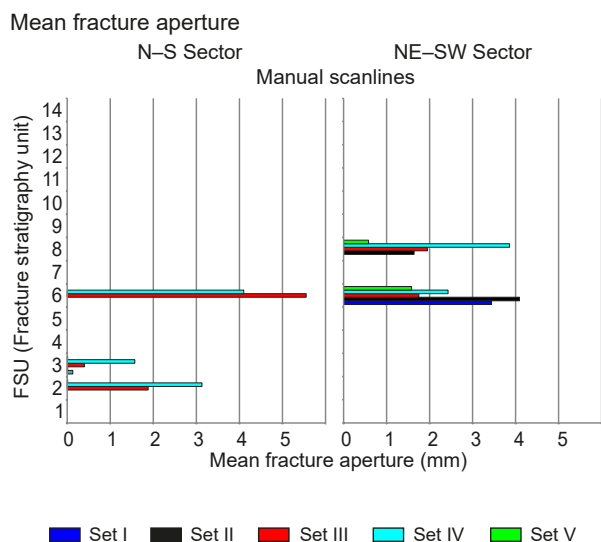
FIGURE 13. Fracture apertures measured in situ during the manual scanlines surveys. Predominantly, the outcrop fractures are in-filled with calcite.

only 10% of the fracture lengths collected via manual scanlines are intact and this remains unknown for SEFL process scanlines, which do not identify fracture tips. The height of the fractures is not dependent on the outcrop orientation but it is controlled by the FSU thickness. Although both height and length have the best-fit with a power law function, the values are only one-dimensional (0.2-3m), which is insufficient to calculate its fractal dimension.

In addition to the coefficients of variation, the fracture spacing (Fig. 7C) measured on the order of decimeters for the dominant fracture sets (*i.e.* I, IV and V), reveals regular spacing without clusters of fractures (Fig. 7D). The cumulative frequency graph of the spacing parameter shows a differentiated exponent for the best-fit function of the Fracture Set I in the N-S sector (Fig. 8). This contrasts with the similarly grouped exponents for the rest of fracture sets due to the favorable orientation of the outcrop for

this measurement. Noteworthy is the low number of high spacing values (>10m), although the methodologies and the HR-DTM have sufficient resolution to measure them. The fracture spacing ratio indicates a low dependence between fracture spacing and FSU thickness which, based on the low fit quality implies that fracture spacing is independent of FSU thickness (Table 1).

The abundance parameter for areal density (P_{20}, Fig. 11A) is higher than for linear intensity (P_{10}, Fig. 7B) for both outcrop sectors due to the increase in the sampling area and the number of fractures involved thus making the result more reliable. However, volumetric intensity results derived from linear intensity (P_{32}, Fig. 12A) are higher than those derived from areal intensities (P_{32}, Fig. 12B), but the values can be considered homogeneous, with some exceptions (FSUs number 10 to 12 in the NE-SW sector). Fracture aperture values measured in manual scanlines (Fig. 13), could allow for the calculation of fracture porosity parameters (P_{11} and P_{33}). However, fractures in the outcrop are infilled with calcite, therefore, sealing the aperture of the fractures. Finally, since fractures are not completely contained within the FSU and exceed the FSU bounds, mechanical layers coincident with FSUs would be interpreted as non-strata-bound, even though they are a small percentage. The fracture system cannot be completely classified as Unbounded (Hooker *et al.*, 2013).

CONCLUSIONS

This work introduces SEFL module III, a software application designed to characterize geometrically the fracture surfaces of a fracture system acquired digitally with remote sensors. The SEFL software workflow includes solutions to individually compute parameters of the characterization, which can be supplemented by classic field sampling methods or vice versa. The goal is to process a large number of fractures to obtain statistically representative and reliable information for the studied outcrop, a task that would be time-consuming to characterize

TABLE 1. Result of the fracture spacing index fit between fracture spacing and FSU thickness (fracture space ratio). Quadratic error values were interpreted as a lack of correlation, suggesting no relationship between fracture spacing and FSU thickness

Fracture Set	Sector N–S			Sector NW–SE		
	Constant	Exponent	Quadratic error	Constant	Exponent	Quadratic error
I	0.0524	0.1601	0.5597	1.3657	0.5631	0.1205
II	1.1672	0.7693	0.0889			
III	1.0214	0.4271	0.0689	0.9032	0.0287	0.0028
IV				1.0541	0.3386	0.1373
V	-0.3729	1.2303	0.7612			

or infeasible through field characterization alone. For this purpose, the software measures parameters such as position, orientation, height, and length, and analyzes them to determine spacing, persistence, and abundance values (Dershowitz and Herda, 1992). If aperture data is available, it also enables the calculation of porosity values.

The resulting data is categorized by fracture sets and computed based on mechanical units defined by the user. Additionally, SEFL software includes a tool that differentiates the rock mass into stratigraphic fracture units based on the intensity of fractures.

The case study of the Añisclo anticline demonstrated the capabilities of the proposed methodology revealing: i) significant real-time saving by the end of the fracture characterization process; ii) comprehensive characterization of the outcrop by remote sensors, as opposed to personal access analysis and iii) increased sampling, leading to greater statistical robustness compared to the limited manual sampling of fractures. Despite the initial time investment, the results are reliable and provide an important geometric fracture characterization of a rock mass. In the Añisclo outcrop SEFL software characterization resulted in 2000 fractures grouped into five fracture sets and 14 FSUs were identified. The computed mean fracture intensity resulted in around 2 to 3 fractures per meter and 4 fractures per square meter, with regular mean spacing and fracture heights around 1m, rarely exceeding 2m. The observed fracture mean length was 2m, considered a minimum length due to the difficulty in observing the full extension of fractures. Five manual scanlines were employed to complement, validate, and compare results from SEFL Module III processing, highlighting the different sensitivities of each technique and the strong dependence of results on the orientation of the measurements. Despite this, combining both methodologies enabled robust results in characterizing the fracture pattern of an outcrop.

Finally, the methodology implemented in SEFL software facilitates the extraction of essential parameters for creating 3D fluid-flow models for hydrocarbon reservoirs, geothermal fields, or numerical simulations when populating models with Discrete Fracture Networks.

ACKNOWLEDGMENTS

CODE AVAILABILITY SECTION

Name of the code/library: Name of the project: Project 120. Name of the application: SEFL software

Contact: e-mail and phone number: dgarcia@ub.edu +34 93 4021378

Hardware requirements: Windows 10. no specific requirements
Program language: Visual Basic
Software required: Microsoft Visual Studio 2017
Program size: 31.7MB

The source code with the Añisclo example and the manuals are available for downloading at the link https://github.com/Geomodels-UB/ and the point cloud can be found in the following link https://dataverse.csuc.cat/dataset.xhtml?persistentId=doi:10.34810/data982

REFERENCES

Arbués, P, Mellere, D., Falivene, O., Fernández-Bellón, O., Muñoz, J.A., Marzo, M., de Gibert, J.M., 2007. Context and architecture of the Ainsa-1-Quarry Channel Complex, Spain. In: Nielsen, T.H. (ed.). Atlas of Deep-Water Outcrops. American Association of Petroleum Geologists (AAPG), Studies in geology, Tulsa (OK), AAPG-Shell Exploration and production, 56, CD-ROM, 1-20. DOI: 10.1306/12401016St563310

Askaripour, M., Saeidi, A., Mercier-Langevin, P, Rouleau, A., 2022. A review of relationship between texture characteristic and mechanical properties of rock. Geotechnics, 2, 262-296. DOI: 10.3390/geotechnics2010012

Assali, P, Grussenmeyer, P, Villemin, T., Pollet, N., 2014. Surveying and modelling of rock discontinuities by terrestrial laser scanning and photogrammetry: Semi-automatic approaches

for linear outcrop inspection. Journal of Structural Geology, 66, 102-114. DOI: 10.1016/j.jsg.2014.05.014

American Society for Testing and Materials, 2005. Standard test method for determination of rock hardness by Rebound Hammer Method, ASTM (D 5873-05).

Bech, N., Bourgine, B., Castaing, C., Childs, J-R., Christensen, N.P., Frykman, P., Genter, A., Gillespie, P.A., Høier, C., Klinkby, L., Lanini, S., Lindgaard, H.F., Manzocchi, T., Middleton, M.F., Naismith, J., Odling, N., Rosendal, A., Siegel, P., Thrane, L., Trice, R., Walsh, J.J., Wendling, J., Zinck-Jørgensen, K., 2001. Fracture interpretation and flow modelling in fractured reservoirs: European Commission Publication, 227pp. ISBN: 92-894-2005-7

Becker, I., Koehrer, B., Waldvogel, M., Jelinek, W., Hilgers, C., 2018. Comparing fracture statistics from outcrop and reservoir data using conventional manual and t-LiDAR derived scanlines in Ca2 carbonates from the Southern Permian Basin, Germany. Marine and Petroleum Geology, 95, 228-245. DOI: 10.1016/j.marpetgeo.2018.04.021

Bertotti, G., Hardebol, N., Taal-van Koppen, J.K., Luthi, S.M., 2007. Toward a quantitative definition of mechanical units: New techniques and results from an outcropping deep-water turbidite succession (Tanqua-Karoo Basin, South Africa). American Association of Petroleum Geologists (AAPG) Bulletin, 91(8), 1085-1098. DOI: 10.1306/03060706074

Bonnet, E., Bour, O., Odling, N., Davy, P., Main, I., Cowie, P., Berkowitz, B., 2001. Scaling of fracture systems in geological media. Reviews of Geophysics, 39(3), 347-383. DOI: 10.1029/1999RG000074

Cooke, M., Pollard, D., 1997. Bedding plane slip in initial stages of fault-related folding. Journal of Structural Geology, 19, 567-581. DOI: 10.1016/S0191-8141(96)00097-1

Corbett, K., Friedman, M., Spang, J., 1987. Fracture Development and Mechanical Stratigraphy of Austin Chalk, Texas. American Association of Petroleum Geologists (AAPG) Bulletin, 71(1), 17-28. DOI: 10.1306/44B4A26C-170A-11D7-8645000102C1865D

Daghigh, H., Tannant, D.D., Daghigh, V., Lichti, D.D., Lindenbergh, R., 2022. A critical review of discontinuity plane extraction from 3D point cloud data of rock mass surfaces. Computers & Geosciences, 169, 105241. DOI: 10.1016/j.cageo.2022.105241

Dershowitz, W., Einstein, H.H., 1988. Characterizing rock joint geometry with joint system models. Springer Rock Mechanics and Rock Engineering, 21(1), 21-51. DOI: 10.1007/BF01019674

Dershowitz, W., Herda, H.H., 1992. Interpretation of fracture spacing and intensity. In: Tillerson, J.R., Wawersik, W.R. (eds.). 33rd U.S. Symposium on Rock Mechanics. Rotterdam, Balkema, 757-766. DOI: 10.1016/0148-9062(93)91769-f

Dershowitz, W., Fidelibus, C., 1999. Derivation of equivalent pipe network analogues for three-dimensional discrete fracture networks by the boundary element method. Water Resources Research, 35(9), 2685-2691. DOI: 10.1029/1999WR900118

Einstein, H.H., Baecher, G., 1983. Probabilistic and statistical methods in engineering geology. Specific methods and examples part I: Exploration. Rock Mechanics and Rock Engineering, 26(1), 39-72. DOI: 10.1007/bf01030217

Ersoy, A., Waller, M.D., 1995. Textural characterisation of rocks. Engineering Geology, 3-4, 123-136. DOI: 10.1016/0013-7952(95)00005-Z

Fernández, O., 2005. Obtaining a best fitting plane through 3D georeferenced data. Journal of Structural Geology, 27(5), 855-858. DOI: 10.1016/j.jsg.2004.12.004

Fernández, O., Muñoz, J.A., Arbués, P., Falivene, O., Marzo, M., 2004. Three-dimensional reconstruction of geological surfaces: An example of growth strata and turbidite systems from the Ainsa basin (Pyrenees, Spain). American Association of Petroleum Geologists (AAPG) Bulletin, 88(8), 1049-1068.

Fernández, O., Muñoz, J.A., Arbués, P., Falivene, O., 2012. 3D structure and evolution of an oblique system of relaying folds: the Ainsa basin (Spanish Pyrenees). Journal of the Geological Society of London, 169, 545-559. DOI: 10.1144/0016-76492011-068

Fisher, N.I., 1985. Spherical Medians. Journal of the Royal Statistical Society, Series B, 47(2), 342-348.

Garcia-Sellés, D., Falivene, O., Arbués, P., Gratacós, O., Tavani, S., Muñoz, J.A., 2011. Supervised identification and reconstruction of near-planar geological surfaces from terrestrial laser scanning. Computers & Geosciences, 37, 1584-1594. DOI: 10.1016/j.cageo.2011.03.007

Garcia-Sellés, D., Gratacós, O., Granado, P., Carrera, N., Muñoz, J.A., Sarmiento, S., Lakshmikantha, M.R., Cordova, J.C., 2018. Fracture analog of the sub-Andean Devonian of southern Bolivia: Lidar applied to Abra Del Condor. In: Zamora, G., McClay, K.M., Ramos, V. (eds). Petroleum basins and hydrocarbon potential of the Andes of Peru and Bolivia. American Association of Petroleum Geologists (AAPG) Memoir, 117, 577-612. DOI: 10.1306/13622135M1173780

Geyer, A., Garcia-Sellés, D., Pedrazzi, D., Barde-Cabusson, S., Martí, J., Muñoz, J.A., 2015. Studying monogenetic volcanoes with a terrestrial laser scanner: case study at Croscat volcano (Garrotxa Volcanic Fields, Spain). Bulletin of Volcanology, 77.22, 1-14. DOI: 10.1007/s00445-015-0909-z

Gigli, G., Casagli, N., 2011. Semi-automatic extraction of rock mass structural data from high resolution LIDAR point clouds. International Journal of Rock Mechanics & Mining Sciences, 48(2), 187-198. DOI: 10.1016/j.ijrmms.2010.11.009

Gillespie, P.A., Howard, C.B., Walsh, J.J., Watterson, J., 1993. Measurement and characterisation of spatial distributions of fractures. Tectonophysics, 226(1-4), 113-141. DOI: 10.1016/0040-1951(93)90114-Y

Gillespie, P.A., Johnston, J.D., Loriga, M.A., McCaffrey, K.L.W., Walsh, J.J., Watterson, L., 1999. Influence of layering on vein systematics in line samples. In: McCaffrey, K.J.W., Lonergan, L., Wilkinson, J.J. (eds.). Fractures, Fluid Flow and Mineralization. London, the Geological Society, 155 (Special Publications), 35-56. DOI: 10.1144/GSL.SP.1999.155.01.05

Gillespie, P.A., Walsh, J.J., Bonson, C.G., Manzocchi, T., 2001. Scaling relationship of joint and vein arrays from The Burren, Co. Clare, Ireland. Journal of Structural Geology, 23(2-3), 183-201. DOI: 10.1016/S0191-8141(00)00090-0

Gross, M.R., 1993. The origin and spacing of cross joints: examples from Monterey Formation, Santa Barbara Coastline, California. Journal of Structural Geology, 15(6), 737-751. DOI: 10.1016/0191-8141(93)90059-J

Hanks, C.L., Lorenz, J.C., Krumhardt, A.P., 1994. Distribution and character of fractures in deformed carbonates of the Lisburne Group, northeastern Brooks Range, Alaska. Geophysical Institute, University Alaska, public-data file 94-19, 26pp. DOI: 10.14509/1705

Hardebol, N.J., Bertotti, G., 2013. DigiFract: A software and data model implementation for flexible acquisition and processing of fracture data from outcrops. Computers & Geosciences, 54, 326-336. DOI: 10.1016/j.cageo.2012.10.021

Hodgetts, D., 2013. Laser scanning and digital outcrop geology in the petroleum industry: A review. Marine and Petroleum Geology, 46, 335-354. DOI: 10.1016/j.marpetgeo.2013.02.014

Hodgetts, D., Gawthorpe, R.L., Wilson, P., Rarity, F., 2007. Integrating digital and traditional field techniques using virtual reality geological studio (VRGS). Society of Petroleum Engineers-69th European Association of Geoscientist and Engineers Conference and Exhibition 2007. Securing the Future, 83-87. DOI: 10.3997/2214-4609.201401718

Hooker, J.N., Laubach, S.E., Marrett, R., 2013. Fracture-aperture size-frequency, spatial distribution, and growth process in strata-bounded and non-strata-bounded fractures, Cambrian Mesón Group, NW Argentina. Journal of Structural Geology, 54, 54-71. DOI: 10.1016/j.jsg.2013.06.011

International Society for Rock Mechanics (ISRM), 1978. International Society for Rock Mechanics, Commission on Standardization of Laboratory and Field Test. Suggested method for the quantitative description of discontinuities in rock masses. International Journal of Rock Mechanics and Mining Sciences and Geomechanics Abstracts, 19, 319-368. DOI: 10.1016/0148-9062(78)91472-9

Jaboyedoff, M., Metzger, R., Oppikofer, T., Couture, R., Derron, M., Locat, J., Turmel, D., 2007. New insight techniques to analize rock-slope relief using DEM and 3D-imaging cloud points: COLTOP-3D software: Rock Mechanics, Meeting Society's Challenges and Demands. Proceedings of the 1st Canada-US Rock Mechanics Symposium, Vancouver, Canada. London, Taylor & Francis, 61-68.

Jones, R.R., Pearce, M.A., Jacquemyn, C., Watson, F.E., 2015. Robust best-fit planes from geospatial data. Geosphere, 12(1), 196-202.

Kulatilake, P.H.S.W., Fiedler, R., Panda, B.B., 1997. Box fractal dimension as a measure of statistical homogeneity of jointed rock masses. Engineering Geology, 48(3-4), 217-229. DOI: 10.1016/S0013-7952(97)00045-8

Lamarche, J., Lavenu, A.P.C., Gauthier, B.D.M., Guglielmi, Y., Jayet, O., 2012. Relationships between fracture patterns, geodynamics and mechanical stratigraphy in carbonates (South-East Basin, France). Tectonophysics, 581, 231-245. DOI: 10.1016/j.tecto.2012.06.042

LaPointe, P.R., Hudson, J.A., 1985. Characterization and interpretation of rock mass joint patterns. Geological Society of America Special Paper, 199, 37pp.

Lato, M.J., Vöge, M., 2012. Automated mapping of rock discontinuities in 3D lidar and photogrammetry models. International Journal of Rock Mechanics & Mining Sciences, 54, 150-158. DOI: 10.1016/j.ijrmms.2012.06.003

Laubach, S.E., Olson, J.E., Gross, M.E., 2009. Mechanical and fracture stratigraphy. American Association of Petroleum Geologists (AAPG) Bulletin, 93(11), 1413-1426. DOI: 10.1306/07270909094

Lei, Q., Latham. J.P., Tsang, C.F., 2017. The use of discrete fracture networks for modelling coupled geomechanical and hydrological behavior of fracture rocks. Computers and Geotechnics, 85, 151-176. DOI: 10.1016/j.compgeo.2016.12.024

Mah, J., Samson, C., McKinnon, S.D., Thibodeau, D., 2013. 3D laser imaging for surface roughness analysis. International Journal of Rock Mechanics & Mining Sciences, 58, 111-117. DOI: 10.1016/j.ijrmms.2012.08.001

Mandelbrot, B., 1982. The Fractal Geometry of the Nature. New York, WH. Freeman and Company, 468pp.

Massiot, C., Nicol, A., Townend, J., McNamara, D.D., Garcia-Sellés, D., Conway, C.C., Archibald, G., 2017. Quantitative geometric description of fracture systems in an andesite lava flow using terrestrial laser scanner data. Journal of Volcanology and Geothermal Research, 341, 315-331. DOI: 10.1016/j.jvolgeores.2017.05.036

Mauldon, M., 1994. Intersection probabilities of impersistent joints. International Journal of Rock Mechanics and Mining Science and Geomechanics Abstracts, 31(2), 107-115. DOI: 10.1016/0148-9062(94)92800-2

Mauldon, M., Dunne, W.M., Rohrbaugh, M.B., 2001. Circular scanlines and circular windows: new tools for characterizing the geometry of fracture traces. Journal of Structural Geology, 23, 247-258. DOI: 10.1016/S0191-8141(00)00094-8

Miller, R.P., 1965. Engineering classification and index properties for intact rock. Doctoral Thesis. University of Illinois, 333pp.

Mochales, T., Casas, A.M., Pueyo, E.L., Barnolas, A., 2012. Rotational velocity for oblique structures (Boltaña anticline, Southern Pyrenees). Journal of Structural Geology, 35, 2-16. DOI: 10.1016/j.jsg.2011.11.009

Muñoz, J.A., 2017. Fault-related folds in the Southern Pyrenees. American Association of Petroleum Geologists (AAPG) Bulletin, 101(4), 579-587. DOI: 10.1306/011817DIG17037

Muñoz, J.A., Beamud, E., Fernández, O., Arbués, P., Dinarès-Turell, J., Poblet, J., 2013. The Ainsa fold and thrust oblique zone of the central Pyrenees: Kinematics of a curved contractional system from paleomagnetic and structural data. Tectonics, 32(5), 1142-1175. DOI: 10.1002/tect.20070

Narr, W., Suppe, J., 1991. Joint spacing in sedimentary rocks. Journal of Structural Geology, 13(9), 1037-1048. DOI: 10.1016/0191-8141(91)90055-N

Nelson, R.A., 2001. Analysis Procedures in Fractured Reservoirs. In: Nelson, R.A. (ed.). Geologic Analysis of Naturally Fractured Reservoirs. Houston, Gulf Publishing, 223-253. DOI: https:10.1016/b978-088415317-7/50008-7

Odling, N.E., 1997. Scaling and connectivity of joint systems in sandstones from western Norway. Journal of Structural Geology, 19(10), 1257-1271. DOI: 10.1016/S0191-8141(97)00041-2

Odling, N.E., Gillespie, P.A., Bourgine, B., Castaing, C., Childs, J-R., Christensen, N.P., Fillion, E., Genter, A., Olsen, C., Thrane, L., Trice, R., Aarseth, E., Walsh, J.J., Watterson, L., 1999. Variations in fracture systems geometry and their implications for fluid flow in fractured hydrocarbon reservoirs. Petroleum Geoscience, 5(4), 373-384. DOI: 10.1144/petgeo.5.4.373

Olariu, M.I., Ferguson, J.F., Aiken, C.L.V., 2008. Outcrop fracture characterization using terrestrial laser scanners: deep-water Jackfork sandstone at Big Rock Quarry. Arkansas, Geosphere, 4(1), 247-259. DOI: 10.1130/GES00139.1

Olson, J.E., Laubach, S.E., Lander, R.H., 2007. Combining diagenesis and mechanics to quantify fracture aperture distributions and fracture pattern permeability. In: Lonergan, L., Jolly, R.J.H., Rawnsley, K., Sanderson, D.J. (eds.). Fractured Reservoirs. London, Geological Society, 270(1, Special Publication), 101-116. DOI: 10.1144/GSL.SP2007.270.01.08

Olson, J.E., Laubach, S.E., Lander, R.H., 2009. Natural fracture characterization in tight gas sandstones: Integrating mechanics and diagenesis: Mechanical and fracture stratigraphy. American Association of Petroleum Geologists (AAPG) Bulletin, 93(11), 1535-1549. DOI: 10.1306/08110909100

Ortega, O.J., Marrett, R.A., Laubach, S.E., 2006. A scale-independent approach to fracture intensity and average spacing measurement. American Association of Petroleum Geologists (AAPG) Bulletin, 90(2), 193-208. DOI: 10.1306/08250505059

Peacock, D.C.P., Nixon, C.W., Rotevatn, A., Sanderson, D.J., Zuluaga, L.F., 2016. Glossary of fault and other fracture networks. Journal of Structural Geology, 92, 12-29. DOI: 10.1016/j.jsg.2016.09.008

Petit, J.-P., Massonnat, G., Pueo, F., Rawnslae, K., 1994. Rapport de forme des fractures de Mode I dans les roches stratifies: Une étude de cas dans le bassin Permien de Lodève (France). Bulletin du Centres Recherches Exploration-Production: Elf Aquitaine, 18, 211-229.

Pollard, D.D., Segall, P., 1987. Theoretical displacements and stresses near fractures in rock, with applications of faults, joints, veins, dikes, and solution surfaces. In: Atkinson, B.K. (ed.). Fracture mechanics of rock. London (England), Academic Press, 277-349. DOI: 10.1016/B978-0-12-066266-1.50013-2

Pollard, D.D., Aydin, A., 1988. Progress in understanding jointing over the past century. Geological Society of America Bulletin, 100(8), 1181-1204. DOI: 10.1130/0016-7606(1988)100<1181:PIUJOT>2.3.CO;2

Priest, S.D., 1993. Discontinuity analysis for rock engineering. London, Chapman & Hall, 473pp. DOI: 10.1007/978-94-011-1498-1

Priest, S.D., Hudson, J.A., 1981. Estimation of discontinuity spacing and trace length using scanline surveys. International Journal of Rock Mechanics and Mining Science and Geomechanics Abstracts, 18(3), 183-197. DOI: 10.1016/0148-9062(81)90973-6

Rios, L.M., Lanaja, J.M., Frutos, E., 1979. Mapa geológico de España 1:50,000. Broto (178, 30-09) sheet, Instituto Geológico y Minero de España (IGME).

Robador, A., Zamorano, M., 1991. Mapa geológico de España 1:50,000. Campo (212, 31-10) sheet, Instituto Geológico y Minero de España (IGME).

Santana, D., Corominas, J., Mavrouli, O., Garcia-Sellés, D., 2012. Magnitude-frequency relation for rockfall scars using a Terrestrial Laser Scanner. Engineering Geology, 145-146, 50-64. DOI: 10.1016/j.enggeo.2012.07.001

Seers, T.D., Hodgetts, D., 2014. Comparison of digital outcrop and conventional data collection approaches for the characterization of naturally fractured reservoir analogues. In: Spence, G.H., Redfern, J., Aguilera, R., Bevan, T.J., Cosgrove, J.W., Couples, G.D., Daniel., J.-M. (eds.). Advances in the study of Fractured Reservoirs. London, Geological Society, 374 (Special Publication), 51-77. DOI: 10.1144/SP374.13

Shackleton, J.R., Cooke, M.L., Sussman, A.J., 2005. Evidence for temporally changing mechanical stratigraphy and effects on joint-network architecture. Geology, 33(2), 101-104. DOI: 10.1130/G20930.1

Slob, S., Hack, R., van Knapen, B., Turner, K., Kemeny, J., 2005. A method for automated discontinuity analysis of rock slopes with 3D laser scanning. January 9-13, Washington DC, Proceedings of the transportation research board 84th annual meeting, 16pp. DOI: 10.3141/1913-18

Smeraglia, L., Mercuri, M., Tavani, S., Pignalosa, A., Kettermann, M., Billi, A., Carminati, E., 2021. 3D Discrete Fracture Network (DFN) models of damage zone fluid corridors within a reservoir-scale normal fault in carbonates: multiscale approach using field data and UAV imagery. Marine and Petroleum Geology, 126, 104902. DOI: 10.1016/j.marpetgeo.2021.104902

Sørensen, E.V., Pedersen, A.K., Garcia-Sellés, D., Strunk, M.N., 2015. Point clouds from oblique stereo-imagery: Two outcrop case studies across scales and accessibility. European Journal of Remote Sensing, 48, 593-614. DOI: 10.5721/EuJRS20154833

Sturzenegger, M., Stead, D., 2009. Quantifying discontinuity orientation and persistence on high mountain rock slopes and large landslides using terrestrial remote sensing techniques. Natural Hazards and Earth Systems Sciences, 9(2), 267-287. DOI: 10.5194/nhess-9-267-2009

Tavani, S., Storti, F., Fernández, O., Muñoz, J.A., Salvini, F., 2006. 3-D deformation pattern analysis and evolution of the Añisclo anticline, southern Pyrenees. Journal of Structural Geology, 28(4), 695-712. DOI: 10.1016/j.jsg.2006.01.009

Tavani, S., Arbués, P., Snidero, M., Carrera, N., Muñoz, J.A., 2011. Open Plot Project: an open-source toolkit for 3-D structural data analysis. Solid Earth, 2, 53-63. DOI: 10.5194/se-2-53-2011

Tavani, S., Granado, P., Corradetti, A., Girundo, M., Iannace, I., Arbués, P., Muñoz, J.A., Mazzoli, S., 2014. Building a virtual

outcrop, extracting geological information from it, and sharing the results in Google Earth via OpenPlot and Photoscan. An example from the Kaviz Anticline (Iran). Computers & Geosciences, 63, 44-53. DOI: 10.1016/j.cageo.2013.10.013

Terzaghi, R.D., 1965. Source of error in joint surveys. Geotechnique, 15(3), 287-304. DOI: 10.1680/geot.1965.15.3.287

Torabi, S.R., Ataei, M., Javanshir, M., 2010. Application of Schmidt rebound number for estimating rock strength under specific geological conditions. Journal of Mining & Environment, 1(2), 1-8. DOI: 10.22044/jme.2011.9

Underwood, C.A., Cooke, M.I., Simo, J.A., Muldoon, M.A., 2003. Stratigraphic controls on vertical fracture patterns in Silurian dolomites, northeastern Wisconsin. American Association of Petroleum Geologists (AAPG) Bulletin, 87(1), 121-142. DOI: 10.1306/072902870121

Van Lunsen, H.A., 1970. Geology of the Ara-Cinca region, Spanish Pyrenees, province of Huesca (with special reference to compartmentation of the flysch basin). Doctoral Thesis. Utrech State University, Geologica Ultraiectina, 16, 119pp.

Wang, X., 2005. Stereological interpretation of rock fracture traces on bore hole walls and other cylindrical surfaces. Doctoral Thesis. Virginia Polytechnic Institute and State University, 113pp.

Warren, J.E., Root, P.J., 1963. The behavior of Naturally Fractured Reservoirs. Society of Petroleum Engineer Journal, 3(3), 245-255. DOI: 10.2118/426-pa

Watlet, A., Triantafyllou, A., Kaufmann, O., Le Mouelic, S., 2016. Comparison of 3D point clouds produced by LIDAR and UAV photoscan in the Rochefort cave (Belgium). Geophysical Research Abstracts, EGU General Assembly, 18, EGU2016-17061-3.

Wilkinson, M.W., Jones, R.R., Woods, C.E., Gilment, S.R., McCaffrey, K.J.W., Kokkalas, S., Long, J.J., 2016. A comparison of terrestrial laser scanning and structure-from-motion photogrammetry as methods for digital outcrop acquisition. Geosphere, 12(6), 1865-1880. DOI: 10.1130/GES01342.1

Wilson, E., Aydin, A., Karimi-Fard, M., Durlofsky, L.J., Sagy, A., Rodsky, E.E., Kreylos, O., Kellogg, L.H., 2011. From outcrop to flow simulation: Constructing discrete fracture models from a LIDAR survey. American Association of Petroleum Geologists (AAPG) Bulletin, 95(11), 1883-1905. DOI: 10.1306/03241108148

Wong, K.W., 1980. Basics mathematics of photogrammetry. In: Slama, C.C. (ed.). Manual of photogrammetry. American Society of Photogrammetry, Falls Church, 37-101. ISBN: 978-0-937294-01-7

Woodcook, N.H., 1977. Specification of fabric shapes using an eigenvalue method. Geological Society of America Bulletin, 88(9), 1231-1236. DOI: 10.1130/0016-7606(1977)88<1231:SOFSUA>2.0.CO;2

Wüstefeld, P., 2018. Structure and diagenesis in Upper Carboniferous tight gas reservoirs in NW Germany. Doctoral Thesis. Karlsruhe Institute of Technology, Karlsruhe (Germany), KIT Scientific Publishing, 144pp. DOI: 10.5445/KSP/1000076144